RESIDUAL STRENGTH ANALYSIS OF AN E GLASS/POLYESTER COMPOSITE SUBJECTED TO IMPACT

A Thesis Submitted to
The Graduate School of Engineering and Sciences of
İzmir Institute of Technology
in Partial Fulfillment of the Requirements for the Degree of

MASTER OF SCIENCE

in Mechanical Engineering

by
Mesut BAYHAN

December 2018

İZMİR

We approve the thesis of **Mesut BAYHAN**

Examining Committee Members:

Prof. Dr. Alper TAŞDEMİRCİ
Department of Mechanical Engineering, İzmir Institute of Technology

Assoc. Prof. Hatice Seçil ARTEM
Department of Mechanical Engineering, İzmir Institute of Technology

Prof. Dr. Meltem Evren TOYGAR
Department of Mechanical Engineering, Dokuz Eylül University

28 December 2018

Prof. Dr. Alper TAŞDEMİRCİ
Supervisor, Department of
Mechanical Engineering
İzmir Institute of Technology

Prof. Dr. Mustafa GÜDEN
Co-Supervisor, Department of
Mechanical Engineering
İzmir Institute of Technology

Prof. Dr. Metin TANOĞLU
Head of the Department of
Mechanical Engineering

Prof. Dr. Aysun SOFUOĞLU
Dean of the Graduate School of
Engineering and Sciences

ACKNOWLEDGMENTS

I would like to express sincere thanks to my supervisor Prof. Dr. Alper TAŞDEMİRCİ and my co-advisor Prof. Dr. Mustafa GÜDEN for their guidance, support and uncomplicated help during my master studies. They significantly extended my knowledge in the field of composites research and opened many doors, which helped to successfully complete and present this document.

I wish to thank my family who deserve a special mention for their endless support and prayers. My father, İbrahim BAYHAN, is the person who helped and directed me during my whole education life to be successful. My mother, Gönül BAYHAN, is the one who sincerely raised me with her caring and gently love. My brothers, Süleyman BAYHAN, Murat BAYHAN, and Mahmut Onur BAYHAN, thank for being supportive.

A special thanks goes to namely Alper CANKAYA, Kıvanç TURAN, Doğuş ZEREN, Semih Berk SEVEN, Çetin UYSAL, Erkan GÜZEL, Fırat TÜZGEL and Fulya AKBULUT for helping me in many ways.

To the team of the Dynamic Testing and Modeling Laboratory, namely, Sevkan ÜLKER, Ayda RAMYAR, Ozan BALYA, Alp Kağan AÇAN, Muhammet ÇELİK, Mustafa Kemal SARIKAYA, and Burak AKYOL, I express my thanks for the supports.

Last but not least, very special thanks go also to the many others that go unmentioned but have contributed in one way or another to the successful outcome of this work.

ABSTRACT

RESIDUAL STRENGTH ANALYSIS OF AN E GLASS/POLYESTER COMPOSITE SUBJECTED TO IMPACT

In this thesis, residual strength analysis of an E-Glass/polyester laminate was carried out for multiple impact loading. MAT_162 material model in LS-DYNA finite element code was used to model the constitutive behavior of the composite and material model parameters were determined using the results of the mechanical characterization. Experimental and numerical multiple loading were performed for two cases, namely Split Hopkinson Pressure Bar (SHPB) and projectile impact testing device. Numerical models were simulated DYNAIN file method strategy in which a composite laminate was impacted multiple times, which was very close to the actual case. A numerical ballistic test model using conventional strategy (in the same simulation all the loads applied sequentially) was employed to check the accuracy of that using the proposed new methodology. After the first hit the SHPB results revealed that delamination occurred at the interface between the first and second layers. Following the second hit, delamination propagated along the inside layers of the composite and occurred at the interface between the eighth and ninth layer. As far as the bar responses concerned, the reflected pulse increased from zero to a maximum value then gradually decreased at the first impact. However, a sharp rise was seen in the reflected pulse of the second impact due to failure corresponding to catastrophic failure. In projectile impact tests, delamination was also found to be increased with the increasing number of hits at both front and back surfaces. Similar results were obtained for both DYNAIN and conventional strategies. It was concluded that simulations showed well agreement with experimental results.

ÖZET

ÇARPMAYA MARUZ BIRAKILMIŞ E CAM/POLYESTER KOMPOZİTİNİN KALICI DAYANIM ANALİZİ

Bu tezde, bir kompozit malzemenin kalıcı dayanım analizi çoklu hasar yüklemeleri için araştırılmıştır. LS-DYNA sonlu elemanlar programındaki MAT_162 malzeme modeli kompozit malzemenin yapısal davranışını modellemekte kullanılmış ve malzeme modeli parametreleri mekanik karakterizasyon sonuçları kullanılarak hesaplanılmıştır. Çoklu yükleme iki durum için gerçekleştirilmiştir. Bunlar Split Hopkinson Basınç Barı (SHBB) ve mermi hasar test düzeneğidir. Numerik modellemede DYNAIN dosya yöntem stratejisi kullanılmıştır. Bu strateji ile kompozit numune deneysel olarak gerçekleştirilen çalışmaya çok yakın bir şekilde çoklu kez hasara maruz kalmıştır. Konvansiyonel stratejinin kullanıldığı nümerik modeller (tüm yüklemelerin sırayla aynı simülasyonda uygulandığı) öne sürülen yeni metodolojinin doğruluğunu kontrol etmekte kullanılmıştır. SHBB testindeki ilk atıştan sonra delaminasyon birinci ve ikinci katmanların arasında ki ara yüzeyde ortaya çıkmıştır. Ancak ikinci atıştan sonra delaminasyon kompozitin katmanları arasında ilerlemiş, ve sekizinci ve dokuzuncu katmanların arasındaki ara yüzeyde meydana gelmiştir. İlk atıştaki bar tarihçeleri incelendiğinde yansıyan dalga sıfırdan maksimum bir değere artmış sonrasında kademeli olarak azalmıştır. Ancak, ikinci atıştaki katastrofik hasardan dolayı yansıyan dalgada keskin bir artış gözlemlenmiştir. Mermi hasar testleri için, delaminasyonun ön ve arka yüzeylerde artan atış sayılarıyla birlikte arttığı bulunmuştur. Benzer sonuçlar hem DYNAIN hem de konvansiyonel metot ile elde edilmiştir. Gerçekleştirilen simülasyon çalışmalardan elde edilen sonuçların deneysel sonuçlarla örtüştüğü sonucuna varılmıştır.

TABLE OF CONTENTS

LIST OF FIGURES

LIST OF TABLES

CHAPTER 1

INTRODUCTION

1.1. Introduction

A blast wave and a blast wind are produced after detonation an explosive weaponry. The blast wave, which occurs a very short time and travels faster than the speed of sound in air, spreads out from the point of source, then compress the air in front of it, causing a nearly immediate increase in pressure. Atmospheric pressure is restored with the passage of the blast wave after the pressure falls away to a negative value. The blast wave reflects from a surface of the structure if it is considered to interact with the surface. Therefore, blast pressure increases at the reflection. Increasing pressure also can be seen when the reflects waves cross (Greaves and Hunt 2011).

The structures can be damaged by overpressure, thermal effects, energized projectiles, debris damage, and cratering and ground shocks which occur subsequent to detonating an explosive device. Since energized projectiles and debris damage produce multi-hit impacts on the structures, they are of the primary interest rather than the others. Energized projectiles are made up of fragments, debris, and missiles which are hurled by the explosive devices while debris damage can be seen in the forms of debris and fragments formed by detonating an explosive weaponry and thrown through the air. Fragments occurred in explosion-related attacks can be classified as the primary fragments that are materials that covered the explosive device and hurled at high speeds following detonation of explosive device and the secondary fragments that are materials that an explosion device is packed with or surrounded by, and thrown by the explosion (Mukherjee et al. 2017).

Fragments created by detonating explosive weapons (bombs, missiles, grenades, land mines, artillery shells, mortars) or Improvised Explosive Devices (IED's) which are packed with nails, ball bearings and glass are considered as a major cause of the casualties in war or populated areas. The number of casualties from the explosive devices is nearly 45624 and 42972 all around the world in 2016 and 2017, respectively. The greater percentage of the injuries and deaths constitute died and wounded civilians and military

personnel from IED's. According to Action on Armed Violence (AOAV), the casualties from IED's are comprised about 29 percent of all casualties in 2006. In Turkey, 4693 civilians and troops were martyred and wounded from explosive violence between 2011 and 2016. Only in 2016, Turkey experienced 2675 deaths and injuries (Dathan 2017). The high number of casualties shows that some precautions must be taken against explosion related attacks. One precaution to be taken against IED's and an explosive device is that military vehicles and body armors must be designed by using advanced armor materials whose mechanical properties are well-known and determined before according to the required test standards.

Figure 1.1. Some types of IED's and corresponding fragments (Source: Moorthy et al. 2014)

Figure 1.2. Fragments occurred following detonating IED's (Source: U.S. Department of Homeland Security Office for Bombing Prevention 2018)

The main point of armor designing is that armor materials must be able to withstand multiple impacts as well as single impact caused by fragments originating from explosive related attacks since each fragment occurred after detonating an explosive device behaves like a projectile, so armor material is subjected to multiple impacts. A few types of IED bomb and fragments created after detonation IED's can be seen in Figure 1.1 and Figure 1.2. IED's also can be packed with nails, ball bearings and glass to increase the lethal effect of impact and induce multi-hit impact on armor by each packed material used (Bors, Cummins, and Goodpaster 2014; Denefeld et al. 2014; Moorthy et al. 2014; Singh et al. 2016). Besides fragments can be produced from closed-range blast loading, the same impact behavior of fragments, multiple impacts, can be seen in this type of explosive device. It is important to know that closed-range blast loading can also accelerate soils that surround or are buried, and the soil particles can behave as fragments and cause the structures in its trajectories to be catastrophically damaged multiple times. The detailed description of closed-range blast loading can be found in literature (Olovsson et al. 2010; Børvik et al. 2011). Moreover, armor itself can cause fragmentation, which is called as behind armor impact. When a projectile impacts an armor, even if it does not complete penetrate the armor, the shock wave occurred can make a piece of the back face accelerate, creating fragments or spalls which can have sufficient velocity to damage armors multiple times. To obtain more information about behind armor impact, it is recommended to investigate literature (Yarin et al. 2000; Arnold and Paul 2001; Arnold and Rottenkolber 2003; Rottenkolber and Arnold 2006). It can be clearly understood from the aforementioned explosion related threats that fragments originating from one of the explosion threats mentioned induce multi-hit impact on armor material and therefore the multi-hit mechanical behavior of armor materials is of primary consideration.

In literature, many studies have been focused on multi-hit impact behavior of composite or other type materials using different types of testing devices and testing methodologies such as low-velocity impact under repeating loads, compression after impact (CAI), multi-hit impact in SHPB and projectile impact tests. In these studies, some authors also tried to validate numerical studies with experimental results, and they wanted to monitor the onset and evaluation of damages occurred after impacts. In these numerical studies, multi-hit impact tests were modeled in a single model file with necessary adjustments for test conditions which were either a certain time interval between projectiles for projectile impact test or the required loading conditions for CAI test. Thus, this methodology having used so far may be insufficient in cases where the number of

impacts is high. Even if it is adequate, modeling multiple impact tests and obtaining results will be complex and take time a lot.

In the study, multi-hit impact models are formed using DYNAIN file method in LS-DYNA. By means of this method, composite materials are impacted multiple times. After a composite specimen is impacted, the damaged composite specimen is written into a file called as a DYNAIN in a simulation file where simulation results are saved. The DYNAIN file consists of the damaged composite specimen with strain and stress. After each impact, it is used as an input for the following impact models. By using this methodology, simulations are modeled in the same way as in experimental studies, and numerical and experimental results can be successfully compared for each impact event. Also, employing this proposed method allows numerical model results to be verified with experimental results after each impact. They are the essential advantages of this method compared to numerical multi-hit impact models having performed using conventional methods until now.

1.2. Literature Survey

Multi-hit impacts on a great variety of material systems can be found in the literature. Because of performing multiple impacts using different testing devices and different impact velocities, the following sections mainly focuses on the review of their experimental and numerical studies.

1.2.1. Low-Velocity Multi-hit Impacts

Some studies have been carried out to investigate the effect of multiple loading at low impact velocity on material strength and behavior such as multi-hit damage response, damage tolerance, flexural strength, and damage resistance. The drop-tower testing machine has been mainly employed in low-velocity multiple loading tests. Found and Howard performed a study on carbon fiber reinforced polymers (CFRP) to investigate the influence of multi-hit loading at below threshold energy values on the damage tolerance and residual strength of composites. Specimens were impacted at 0.54 J (100 impacts) and 0.73 J (33 impacts) as well as being impacted by a single impact. It was found for the single impact events that the impact force had more the effect on the initiation of failure

compared to the impact energy. They reported that there were no important changes in the impact force obtained from the multiple impacts in contrast to the first impact. 0.93 J impact energy caused the impact force with increasing impact duration to a significant reduction (Found and Howard 1995).

The effect of impact energy and multi-hit impacts on the flexural strength and interlaminar shear strength of stitched and non-stitched glass reinforced composite laminates was investigated by Mouritz et al. Kevlar thread was used to stitch the fibers through the thickness with a low or high stitch density. It was found that the flexural and interlaminar shear strength decreased with increasing number of repeated loading, and dominant failure modes were shear cracking of the resin, delaminations, and crushing and fracture of fiber materials. It was also found out that the effect of the delamination damage on stitched composite laminates was more than on unstitched composite laminates (Mouritz, Gallagher, and Goodwin 1997).

Hosur et al. carried out a study on stitched and unstitched S2-glass/epoxy composites to elucidate the damage resistance of these composite materials subjected to multiple impacts. It was observed that all composite laminates subjected to multiple impacts withstood a certain loading at energy levels up to 30 J while at energy levels 40 and 50 J, the failure of stitched composite laminates took place in a smaller number of impacts than stitched composite laminates. It was also found that at lower energy levels, the peak loads obtained from repeated loading did not change while at higher energy levels, they decreased suddenly after certain impact numbers. When the results obtained from the tests were compared in terms of absorbed energies, their values did not show significant changes between all repeated impact conditions. When being taken into consideration the results obtained for damaged areas, they increased with increasing number of impacts. Then, after certain impacts, there was no significant change in damage regions (Hosur, Karim, and Jeelani 2003).

Sugun and Rao argued the influence of multiple loading on the behavior of composite laminates consisting of glass/epoxy, carbon/epoxy and kevlar/epoxy using a drop-weight testing machine. They figured out that the peak load decreased with increasing number of impacts while the total energy increased until fracture. Also, they proposed and verified an arithmetic relationship between incident energies and number of impacts to failure. Number of damages to failure was determined and extrapolated using the proposed relationship to decrease material costs, fabrication costs, testing costs

and time. The relationship was found to be very useful to provide an information about the damage tolerance of composites (Sugun and Rao 2004).

De Morais et al. argued the laminate thickness effect on the multi-hit damage resistance of glass/epoxy, carbon/epoxy and aramid/epoxy composite materials using a drop-tower testing machine. They reported that the laminate thickness was the most important parameter to determine the impact resistance of the composites impacted below a certain impact energy level. For higher impact energy levels, the fiber material and laminate thickness are found to have a significant effect on determining the impact resistance of composites (De Morais, Monteiro, and d'Almeida 2005a). In a follow-up study, the influence of low-velocity multiple impacts on the performance of carbon-epoxy composite laminates was investigated. Different types of stacking sequences were selected to manufacture carbon-epoxy composites, namely unidirectional laminate, cross-ply laminate, and non-symmetric laminate. Their study revealed that the performance of cross-ply and non-symmetric composite laminates against low-velocity impacts is better than that of unidirectional composite laminates since these composite materials consist of multidirectional reinforcements. It was also found that for the composite laminates with multidirectional reinforcements, crack paths were restricted because of the fiber architecture of these composite laminates. For the unidirectional composites, cracks can propagate easily, causing the composites to fast failure (De Morais, Monteiro, and d'Almeida 2005b).

Chakraborty and Kumar studied the influence of simultaneous and sequential multiple impacts on the impact response of unidirectional graphite/epoxy composite laminates using finite element analysis. They reported for simultaneous multiple impact scenarios that delaminations were initiated from the impact region, and then it formed one big delamination with increasing impact velocity. It was reported for sequential multiple impact scenarios that as the time between the first and second impact increased, so did magnitude of contact force. However, the delamination regions occurred after sequential impacts did not extend and form one big delamination with increasing time interval between sequential impacts. When sequential impacts were struck quickly, the delamination regions formed one big delamination (Chakraborty and Kumar 2005).

The influence of manufacturing methods on the response of thick glass reinforced plastic composite laminates against multiple impact loading was investigated by Belingardi et al. using a drop tower testing machine. The composite materials fabricated using hand lay-up and vacuum infusion techniques were impacted up to 40 times or

perforation. It was found that for non-perforation impact events there were not seen any significant changes in force and energy curves, and damage parameter while for perforation impact events the composite laminates fabricated using hand lay-up withstood more impacts than those fabricated using vacuum infusion (Belingardi, Cavatorta, and Paolino 2008).

David-West et al. carried out a study on balanced laminates, namely symmetric, antisymmetric and asymmetric to determine the behavior of these composite laminates subjected to multi-hit impacts using a drop weight testing device. The results revealed that stacking sequence and crack path had a significant effect on the damage resistance of composite laminates. It was also found out that symmetric laminates showed the greatest strength against multi-hit impacts, and the main failure mode occurred in the perforated side of composites was found to be matrix cracking and back face splitting (David-West, Nash, and Banks 2008).

Azouaoui et al. conducted a study to investigate the fatigue behavior of glass/epoxy cross-ply composite laminate subjected to multi-hit loading. After impacting the center point of a composite plate multiple times, a crater occurred at the impact face of the composite plate due to crushing and deforming of the internal plies below the impact point. The process forming the crater carried on with increasing number of impacts, and it was completed when the composite laminate was completely penetrated. Delamination occurred within composite laminates in the direction of the fibers in the bottom ply of the composites. It was found to be the main failure mode. Moreover, a damage parameter was defined as a scalar variable that characterizes material damage. They reported the damage parameter versus number of impacts plots for the tests performed. In these plots, three distinct regions were obtained. It was found that in the first region the plate stiffness decreased with increasing number of impacts, in the second region the residual stiffness and damage parameter did not change with increasing number of drops, and in the third region this phase ended with the failure of the composite laminate, and during this phase a little over 80% of the remaining damage was consumed (Azouaoui, Azari, and Pluvinage 2010).

The influence of multi-hit impacts on the fatigue behavior of self-reinforced polypropylene composite laminate was investigated by Aurrekoetxea et al. using a falling weight testing device. They reported that during impacts, laminates underwent plastic deformation. After being penetrated composite, a localized star-shaped hole was seen on the back side of the laminate. Moreover, it was found that there were not seen any sign of

plastic deformation of laminate up to 5 J. However, after 5 J impact energy level, permanent deflection increased with increasing impact energy level up to the that occurred penetration (13 J). Also, it was found out that the maximum number of impacts penetrating laminate dropped suddenly because of taking place the fiber breakage after the plastic deformation, and this caused the fatigue life of laminate to decrease. Furthermore, the amount of absorbed energy decreased after laminate underwent plastic deformation, and it increased after the fiber breakage took place (Aurrekoetxea et al. 2011).

1.2.2. Compression After Impact Tests

CAI tests have been performed to examine CAI strength or damage tolerance of materials and to characterize damage. In this method, the drop-tower testing machine was first used to induce impact on composite materials. Then, the pre-impacted composite materials were subjected to compression loading. Therefore, they were exposed to multiple impacts. In the numerical models of this test, simulation has been modeled as multiple steps. In the first step, materials were impacted with an impactor at low impact velocities. At the end of the step, the impactor was withdrawn from the simulation. Before quasi-static compression steps, there was a pause step. In this step, required boundary conditions were redefined, then the pre-impacted materials were compressed at quasi-static strain rates to determine the residual strength of materials.

Jones performed a study on graphite/ epoxy composite materials. The composites were impacted single and multiple times using ball bearings, then compressed via a static compression testing device. The pre-damaged samples were repaired after single and multiple impacts to investigate the effect of repairing on their compression strength. They performed impact tests at low-energy impact level since they proposed that the problem of low-energy impact damage was of particular concern due to a decrease in the compressive strength of composite samples. It was concluded that in order to repair the impacted specimens an externally bonded can be used quickly and easily (Jones 1994).

Xiong et al. developed an analytic method to determine the CAI strength of composite laminates impacted using a drop weight testing machine. The decrease in elastic moduli of composites was calculated by a sublaminate buckling analysis while the stress distribution in damaged specimens was determined to employ a complex potential

method. The residual compressive strength of composites was calculated from stress results. The results obtained from the experimental studies were also used to validate the numerical results. It was found out that the buckling stress was sensitively affected by the out-of-plane deformation and decrease in bending moduli of sublaminate because of asymmetric lay-up (Xiong et al. 1995).

De Freitas and Reis devoted a study on carbon fiber reinforced epoxy composite materials to obtain the damage growth mechanism. They were impacted and then compressed by using an instrumented and a modified the drop weight testing machine. The composite laminates with 24 plies were comprised of a different number of interfaces, and they were produced using carbon fibers with four stacking sequences and two different epoxy resins. The composites were first impacted at the Barely Visible Impact damage energy level (BVID) and then compressed following being prepared according to the proposed standards. The effect of the number of interfaces on the delaminated area owing to impact loading was found to be much greater than the examined stacking sequences. A buckling mechanism in the delaminated area caused unstable damage growth obtained by compression after impact. The delaminated area and the distance between the delaminated area and the lateral borders affected the residual strength (De Freitas and Reis 1998).

Hawyes et al. conducted a study on intact and damaged carbon fiber/epoxy composites with 4-, 6- and 8-mm thickness. They were impacted at and above threshold energy to obtain their CAI strength by means of a new CAI Rig. The intact specimens were used to determine their failure load and strain under compression using the CAI Rig. Also, strain gages were attached to composite laminates to obtain strain data. The load-strain curves of 4- and 6-mm plates obtained from compressing the plates showed that the initial linear region of curves was followed by a non-linear behavior. Also, decreasing one strain gage while increasing the other was suggested an overall buckling of composite laminates. It was found from the study that the CAI strength of 4- and 6-mm plates were not affected at threshold impact energy. With increasing the level of the threshold impact energy, the CAI strength of the plate in 4 mm thickness decreased while that of the plate in 6-mm thickness increased (Hawyes, Curtis, and Soutis 2001).

Naik et al. attempted to determine the effect of the plate thickness on compression after impact behavior of plain weave fabric E-Glass/Epoxy composite plates whose thicknesses were 8 mm, 6.4 mm, 5 mm and 4.4 mm. Damage area due to impact was also examined for the upper and lower surface of the composite plates. It was found that the

damaged area was the quasi-lemniscate shape on the upper surfaces while being the circular shape on the lower surfaces of the composite plates. For the higher plate thickness, damage due to impact did not spread throughout plate thickness because impact energies were absorbed by local indentation or crack formation on the upper surface. The intensity of damage was more on the upper surface than on the lower surface. For the lower plate thickness, the impact energy absorbed by plate deflection and fracture energy was found to be less, and damage propagated throughout the plate thickness. The intensity of damage was more on both the upper surface and bottom surface for this case. Damage tolerance was determined from the ratio of the post-impact compressive strength to the compressive strength of the intact composite. The damage tolerance of the lower plate thickness was found to be less while that of the plate with a higher thickness was more. Therefore, residual strength increased with increasing plate thickness. They also obtained that the failure mode of composites was shear failure for all cases, the maximum damage area was seen in the plate thickness of 5.0 mm (NAIK et al. 2004).

Sanchez-Saez et al. examined the damage tolerance and residual strength of various lay-ups of the carbon fiber/epoxy laminates which were made of 2.2 mm thick woven laminate (10 plies), 2.2 mm thick cross-ply laminate ($[0/90]_{3s}$) and 1.6 mm thick quasi-isotropic laminate ($[45/0/90]_s$). They used a drop weight test machine for impacts. For compression tests, they developed a new testing device where the usage of tabs and any changes in the specimen geometries were not needed. To a better understanding of the behavior of laminate lay-ups, different impact energies were selected. When the amount of absorbed energy of carbon fiber/epoxy composite laminates was similar, the damage area in the cross-ply and quasi-isotropic laminates were found to be the same. It was the largest in woven laminates due to being prevented the propagation of the shear cracks and delamination by the weave structure of the reinforcement. The residual strength of woven carbon fiber/epoxy composites was found to be greater than the others under all the impact energies while that of quasi-isotropic laminates was the lowest. Besides the damage tolerance of quasi-isotropic laminate was the best because the reduction of the normalized strength of quasi-isotropic laminate was the smallest at all levels of impact energies applied (Sanchez-Saez et al. 2005).

Yan et al. investigated the CAI strength of woven E-glass fiber reinforced vinyl ester composites. They found that delamination propagated across the width of the specimen between middle-plies, and it initiated the sublaminate buckling. In addition to these findings, matrix and fiber cracking occurred at the back side of the specimen upon

sublaminate buckling. They propagated laterally and along the thickness direction in shear mode, causing the specimens to fail ultimate strength under compressive loading (Yan et al. 2010).

Ghelli and Minak performed drop-weight tests and compression after impact tests on carbon fiber reinforced epoxy composite materials. To investigate the effect of specimen geometry (rectangular and circular) and stacking sequences on impact and post-impact response, several tests were conducted. Due to being different of specimen dimensions and geometries, different impact response and damage were obtained. The delamination in the specimen with circular shape extended more areas than that in the specimens with a rectangular shape. Furthermore, it was observed that different material response was seen in the rectangular samples due to the lay-up. Moreover, test configuration and stacking sequences were found to have no effect on the relationship between delamination area and absorbed energy, and between delamination area and maximum contact force (Ghelli and Minak 2011).

A numerical model was developed by Caputo et al. to enhance damage resistance of composite structures. The developed model was used to simulate the impact event so as to observe damage initiation and propagation of interlaminar and intralaminar damages. Moreover, it was used to interpret the quasi-static compressive behavior of intact and impacted composite structures (Caputo et al. 2014).

A new compression after impact device was developed by Remacha et al. to investigate compression after impact strength of laminate materials. The thickness of composites was selected to be less than that recommended by CAI test standards. In order to verify the accuracy of the new device, laminate plates were tested using both test fixture, namely the standard test and new test fixture. It was found that the test results obtained using the new CAI device were similar to those obtained using ASTM test fixture (Remacha et al. 2015).

Caputo et al. conducted an experimental and numerical study on composite materials made of carbon fiber reinforcement material and the RTM6 resin material to investigate impact damage growing mechanisms. The composite specimens were impacted at different impact energy levels and then subjected to compressive loading. ABAQUS finite element code was employed to model the CAI experiments. Besides the numerical model was formed using one model file where different boundary conditions were described for low-velocity impact and compression tests. After conducting the impact and CAI tests on the composite materials, their results showed that the damage

evolution and residual strength of damaged composite materials in the numerical model well agreed with those obtained from the experimental study (Caputo, De Luca, and Sepe 2015).

Han et al. carried out an experimental and numerical study on composite laminates (CCF300/Epoxy, CCF300/Bismaleimide, CCF800/Epoxy, and CCF800/Bismaleimide) to determine damage tolerance of these composite materials. They struck the composites at low impact velocity and then compressed using CAI device. Moreover, the intralaminar damage and interlaminar delamination were investigated using ABAQUS finite element code. They proposed a finite element model consisting of a novel multi-scale failure criterion (MMF3) and cohesive elements. By means of the experimental and numerical studies, it was observed that for all types of composite materials, higher maximum impact contact force and shorter impact duration, and more serious interlaminar damage and larger dent depth are obtained at larger impact energy level. It was also found that CCF300/Epoxy laminates showed a better damage tolerance performance than CCF300/Bismaleimide laminates. Besides CCF300 carbon fibers showed better damage tolerance, compared to CCF800 carbon fiber reinforcements. The numerical results were found to corroborate with the experimental results (Han et al. 2016).

An integrated numerical model without major simplification and idealizations of damage in composite materials was examined by Abir et al. to determine the influence of impact damage on strength of composite materials. They figured out that after impacting the composite material, the buckling caused by impacts triggered the damage growth through CAI, and it resulted in fiber and delamination damage growth, leading to rapid and sudden load drops. It was also found out that Mode I fiber compressive fracture toughness and Mode II interlaminar fracture toughness had an important effect on the residual strength of composite materials (Abir et al. 2017).

1.2.3. Multi-hit Impacts in Split Hopkinson Pressure Bar

Studies on multi-hit impact tests in SHPB have been conducted experimentally to determine reductions in strength or residual strengths of materials using consecutive stress pulses, stuffed striker or striker bars with different materials. In the case of using the split Hopkinson tensile bar (SHTB), Shim et al. proposed a method to deform polymer materials using two-stage dynamic-dynamic tensile pulse. The rate-independent LEXAN

141 polycarbonate was first used to validate the proposed method via quasi-static and dynamic two-stage loading, experimentally and analytically. The aforementioned method was based on a technique by which a specimen loaded using the initial incident wave, and briefly unloaded, then reloaded until fracture. In the first stage of the loading, an input tensile wave was generated using a simple pendulum striker and a corresponding stress-strain curve was determined from the classic split Hopkinson tension bar method whereby the strain and strain rate and stress in the specimen were determined from the reflected wave and transmitter wave, respectively. They determined the second-stage incident wave by employing the following two assumptions: First, the transmitter wave was the algebraic sum of the incident and reflected waves. The other, there was no any distortion of propagation of stress pulses along the bars and reflected pulses from free ends. Based on these assumptions, they determined the dynamic stress-strain curves for one and two-stage loading, and they checked the results obtained from the dynamic two-stage loading against that obtained from the static two-stage loading. Then, they found that the static and dynamic stress-strain curves showed well agreement with each other, and the proposed method can be used to determine the dynamic behavior of rate-dependent polymer materials (Shim, Yuan, and Lee 2001).

Chen and Luo performed the study on ceramic specimens to understand the dynamic compressive behavior of them. They improved the conventional split Hopkinson bar technique using two consecutive stress pulses. The behavior of the intact ceramic specimen at high strain rate was determined from the first loading pulse while the dynamic compressive constitutive behavior of the damaged ceramic specimen was obtained from the second loading pulse. The pulse shaper was used in the tests in order to deform ceramic specimens at nearly constant strain rates under dynamic stress equilibrium. It provided controlling the amplitudes of loading pulses, the values of strain rates, the maximum strains in the ceramic specimens, and the proper separation time between the two loading pulses. They tried to obtain information about the penetration resistance of the ceramic target used in armor systems. They reached the results from three tests that the first loading pulse deformed and crushed the intact ceramic specimen at about 170 s^{-1} strain rate while the second loading pulses deformed the damaged ceramic specimens at about 83,174 and 517 s^{-1} strain rates (Chen and Luo 2004).

Chen et al. conducted an experimental study using a modified split Hopkinson test technique to determine the dynamic compressive response of hot-pressed silicon carbide (SiC-N) as a function of loading rates, damage, and confinement. In this technique, the

striker bars were connected with a spring, resulting in the pulse delay. Two consecutive stress pulses generated by the strikers in a single dynamic experiment were used to load the intact and damaged ceramic specimens. The response of the ceramic specimens against the pulses was calculated. The first pulse first characterized the intact ceramics, then crushed it into a comminuted state while the second pulse determined the dynamic constitutive behavior of the damaged ceramic. It was reported that the first pulses crushed the intact ceramic specimens at the strain rates between 325 and 500 s^{-1} at 26 MPa of confining pressure, generating the peak stress varied between 5 and 6 GPa. Since the quasi-static compressive strength was varied between 4.9 and 7.1 GPa, they found that rate effect was less important than the scatter in data. For the second loading with the strain rates varied from about 800 to 1700 s^{-1}, the strength of the damaged SiC-N was not the strain rate sensitive owing to the stress-strain curves of the ceramic overlapped. The same behavior was seen in the stress-strain curves of the damaged ceramic at 56 and 104 MPa of confining pressure. When the effects of confinement examined at similar strain rates, the stress-strain curves of the damaged ceramic showed almost linear hardening at 26 and 56 MPa confining pressure while it showed non-linear hardening at 104 MPa confining pressure. The results obtained from examining the effect of damage on mechanical behavior of the ceramic indicated that there was a critical level, and the specimen behaved very rigid below that level while the second loading pulse occurred at a much higher strain rate beyond that level, and the damaged ceramics showed rate-independent behavior after that level reach (Luo, Chen, and Rajendran 2006).

Rachel et al. modified the conventional SHPB to deform a BCC metal (iron) and an FCC metal (copper) at different strain rates using a striker bar. The striker bar was assembled two rods of materials which have different mechanical impedances. Therefore, step-down or step-up loading pulses were readily produced depending on where the higher impedance material was used. A step-down loading pulse was obtained when the higher impedance material stuck first the incident bar, while a step-up loading pulse occurred when the lower impedance material struck first the incident bar. They preferred the step-down pulse in the experiments because the step-up pulses made the duration of the incident pulse too long and caused the yielding to happened after the transition of pulses happened. Maraging steel was selected as the higher impedance material while Dural was selected as the lower impedance material. They conducted experiments on the specimens using step-down pulses. Using equivalent strain rates calculated from step-

down pulses, single-rate experiments were also performed to verify the behavior of materials under these strain rates. (Briggs et al. 2007).

Chen et al. examined a modified stuffed striker in a classical SHPB to investigate the dynamic mechanical behavior of rate-dependent materials. They implemented a stuffed striker to the conventional SHPB. The stuffed striker was utilized to double stress. It was made up of a striker tube, a striker bar and a gap which was a clearance between the inner surface the front cap of striker tube and the front end of striker bar inside the striker tube. The gap ensured the time delay between the first pulse and second pulse and the proper pulse separation. The modified technique was also combined with the Lindholm technique to obtained triple or more loading pulses. In their study, the modified split Hopkinson technique was employed in investigating the mechanical behavior of polycrystalline Cu at high strain rates. They demonstrated that the proposed SHPB technique was used to validate experiments conducted on polycrystalline Cu and to obtain the dynamic behavior subjected to double and triple loading pulses, precisely (Xia et al. 2008).

1.2.4. Multi-hit Projectile Impact Tests

Authors examined multiple impact tests on composite materials using a projectile impact testing device to determine their ballistic limit and ballistic performance. In this testing method, single impacts were performed on composites to determine their ballistic limit velocity. To determine damage tolerance and changing in ballistic limit velocity, additional impacts were conducted on damaged composite laminates. In numerical studies, a certain time interval between projectiles were used to obtain multi-hit impacts in one simulation file.

Deka et al. carried out an experimental and a numerical study on S-2 Glass/SC15 epoxy composite laminates to determine the effect of sequential and simultaneous multi-hit high velocity impacts on the ballistic performance of the composite laminates in terms of energy absorption, new surface creation, and failure mechanisms. Finite element modeling (LS-DYNA 3D) was used to provide insight into failure modes, energy absorption, and damage prediction. In the numerical models, the projectiles were placed 0.04 mm away from the composite so as to minimize the simulation time for simultaneous impact scenario while a distance of 50 mm between the projectiles was used to model for

the sequential impact scenario so as to decrease stress wave interaction. The new surface creation in the specimen impacted sequentially was found to be more than that impacted simultaneously. Also, it was also found that for both sequential and simultaneous impacts, the energy absorption ability of the composite laminates decreased with an increase in the number of impacts due to a decrease in contact stiffness after each impact, causing in an increase in exit velocity (Deka, Bartus, and Vaidya 2009).

Perez-Martin et al. conducted a study on hybrid woven carbon and S2 and E glass fabric laminates to determine the behavior of composite materials subjected to multi-hit impacts. It was found that if the distance between the impacts is less than 6.3 mm the ballistic performance of composite laminates will be affected by each impact, while if the distance between the impacts is more than 7.5 mm there will not any effect of the impacts on the ballistic performance of composite laminates. It was also found out that the residual velocities of the projectile increased with increasing impact velocities (Perez-Martin et al. 2012).

The influence of support spans on single-hit penetration resistance and the influence of multi-hit impacts on the multi-hit ballistic limit for S-2 glass/SC15 composite plates were investigated by Haque et al. experimentally. To investigate the influence of support on single-hit penetration resistance, single-hit ballistic tests were performed. Besides multi-hit impacts were performed on composite plates by impacting at additional impact locations to investigate the influence of multi-hit impacts on the multi-hit ballistic limit. Their study showed that for the single-hit impact condition the ballistic limit velocity increased with support span diameter, and the damage induced on the specimen extend throughout the edges of support spans. It was also found from the experimental study that for multi-hit impacts the ballistic limit velocity of composite plate decreased due to pre-existing damage (Haque, Harrington, and Gillespie 2012a). The numerical study was conducted to verify and compare the results obtained from simulation and experiment using finite element code software (LS-DYNA). The simulation was modeled using three-dimensional solid elements, and it was formed a single model file in which the composite laminates were impacted at additional five different impact locations using fragment simulating projectiles at an interval of 200 microseconds. It was found out that ballistic limit velocities obtained from the numerical study well correlated with that obtained from the experimental studies. It was also found that when being impacted on a damaged composite laminate, the local transverse shear stiffness was lowered, causing the penetration resistance of the composite material to decrease. Therefore, the composite

plate was completely penetrated at velocities below the single-hit ballistic limit (Haque, Harrington, and Gillespie 2012b).

Kong et al. developed a new method called as Geometric Intervals Method (GIM) in a numerical model to impact on $AL_2O_3/Al2024$ composite laminates in multiple times using armor piercing projectiles (APPs). In this method, the bullets were spaced the equal time interval, and they were triggered at the same time to impact into the composite laminates, so the composite materials were subjected to multiple impacts. The debonding of ceramic tiles were predicted successfully by the developed method, and the numerical model correlated well with experiments with regard to debonding of the ceramic tiles for all cases (Kong, Jiang, and Liu 2012).

Naebe et al. performed an experimental study on a new composite material made of polymer resin and ceramic particulate to examine the ballistic performance of the composite material against fragment simulating projectiles (FSPs). Their study showed that the amount of damage on the composite laminates impacted in multiple times was 2-3 times the projectile diameter. The cracks occurred after impact extended between impact sites. It also found that the novel composite material used in the study had more damage tolerance than traditional sintered ceramic materials, and the proposed material had an advantageous multi-hit capability (Naebe et al. 2013).

Jover et al. examined the response of balsa core sandwich composite with thin carbon fiber skins against multi-hit sequential ballistic impacts. It was found that the response of composite laminates against the prior impacts in terms of residual and absorbed energies was very noticeable as number of impacts increased. However, a limited effect of repeated impacts on the global response of this type of the composite material appeared at the end of the study (Jover, Shafiq, and Vaidya 2014).

The multi-hit impact behavior of a hybrid composite armor material consisted of ceramic and fibrous content was investigated by Fejdys et al. according to the standard test methods. They found that damage occurred within the composite laminates due to the multiple impacts increased the severity of damage because of the short distances between the damaged regions on the composite laminates. Moreover, using a suitable confinement system, the protective properties of the composite laminates were improved at a certain amount comparing to the composite laminate without the system confinement (Fejdys et al. 2016).

Prakash et al. conducted a study on steel fiber reinforced cementitious composites (SFRCC) to determine the multi-hit behavior of the composites, and to simulate the multi-

hit impact events on the composites. In the numerical models, a time delay of 200 μs was used between projectiles so as to form the two consecutive impacts on the composite. This time delay was selected by taking into consideration transferring time of the all kinetic energy of the projectile to the composite. It was also ascertained that when the distance between the impact points is more than ten times of the diameter of the projectile, the impact event is called as single-hit impact condition (Prakash, Srinivasan, and Rao 2017).

Garzon-Hernandez et al. performed an experimental study on short carbon fiber reinforced PEEK to determine the response of the mechanical behavior of the composite laminates against multi-hit high-velocity impacts which consisted of sequential and simultaneous impacts. They also obtained information about the effect of these impact scenarios on the energy absorption, damage extension, and failure mechanisms within the composite materials. It was found for the sequential impacts that when the composite laminates were impacted a subsequent projectile, a reduction in the ballistic limit was observed. The composite laminates failed catastrophically after the subsequent impacts since the pre-damaged regions in the composites were triggered and affected by the subsequent impact. Moreover, for the simultaneous impact events, the interaction between cracks propagation, stress waves and complex bending effects were found. Using the combined influences of this interaction, the damage mechanisms and the damage extent were ascertained (Garzon-Hernandez, Garcia-Gonzalez, and Arias 2018).

1.3. Aim and Scope of the Study

As mentioned before, explosive-related threats can cause fragmentation and spall effects. These fragments or shrapnel may impact on composite materials used as spall liners or armor materials multiple times. Thus, multiple impact studies are of primary interest to provide protection, and to take precautions against these threats.

The thesis first aims to provide a new numerical technique which makes multi-hit impact simulation of an E-Glass/Polyester composite material easier and reduces computation time. The second aim is to characterize the mechanical behavior of the composite and determine its material model parameters through quasi-static static and high strain rate tests.

In the study, the residual strength of an E-glass/polyester composite material has been investigated experimentally and numerically. In experimental studies, quasi-static tests encompassed compression, tension, V-notched, laterally constrained compression, and elastic constant determination tests while dynamic tests involved split-Hopkinson pressure bar and projectile impact tests. Although DYNAIN file method has been only used for forming simulation until now, it has been utilized to investigate the multiple loading behaviors of composite laminates in this study. Hongang et al. performed a study on the modeling of pre-bending simulation of a tube, and DYNAIN file obtained used SPRINGBACK-LSDYNA keyword in LS-DYNA was further utilized to improve hydroforming process (An et al. 2013). A numerical study was also carried out by Tasdemirci et al. to simulate a deep-drawing process using the same method. They suggested that shell geometries may maintain important amount of residual stress and strain after the deep-drawing process. Then, the shell geometries with residual stress and strain were used in numerical quasi-static and dynamic crushing simulations (A Tasdemirci et al. 2015; Alper Tasdemirci et al. 2015). When studies related to multiple impacts are reviewed, it can be found that the numerical study of multi-hit impacts on composite materials is not enough to characterize the multi-hit behaviors of composite materials under multiple loading. To the author's knowledge, this is the first study examining the multi-hit impact behavior of composite materials in numerical models using DYNAIN file method. The method having used in forming simulations so far has been examined to model two multi-hit impact cases. The first case is multiple loading in SHPB, the second one is multi-hit impact studies on composite materials in projectile impact tests By employing this method, the failure modes of composite materials have been clearly monitored following each impact such as matrix failure, delamination, and fiber fracture. This plays an important role in investigating the behavior of composite materials under multiple loading.

The presented study consists of five chapters. In the first chapter, there is a brief background about the performed study, and some of the threat types and the effects of them on the composite material used as an armor material on the inside or hull of the vehicle are introduced. Then, some studies performed to investigate the multi-hit capacity of composites laminates using the different testing device are explained. In the second chapter, the fabrication of the composite laminates is briefly explained, and the quasi-static and dynamic characterization tests conducted to determine MAT_162 material model parameters according to standard test methods are mentioned. Also, the steps

followed in the multiple impact experiments are told. In the third chapter, the failure mechanisms in MAT_162 composite material model are mentioned. The numerical models used for the calibration of the quasi-static and dynamic tests are explained in detail, and the multi-hit impact models are told, too. In the fourth chapter, the results obtained from the experimental characterization and multi-hit impact tests are compared to the results obtained from the numerical calibration and multi-hit impact models. In the fifth chapter, the conclusions are given.

CHAPTER 2

EXPERIMENTAL METHODOLOGY

2.1. Introduction

In this chapter, firstly manufacturing method of a cross-ply E-glass fiber reinforced polyester resin composite material in $[0/90]_s$ fiber orientation was mentioned in detail. In numerical models, MAT_162 material model was selected to investigate the onset and evaluation of damage within composite materials, and the required parameters for this material model and corresponding the standart test methods were summarized in Table 2.1. Some of these parameters were determined from corresponding standard test methods while the others were calculated from numerical studies. The tests performed at low and high strain rates to characterize the mechanical properties of composite materials were introduced in the following sections. For quasi-static strain rate tests, Shimadzu testing machine was employed while high strain rate tests were conducted in SHPB. In-plane tensile tests, V-Notched beam tests, elastic constant determination tests, and laterally constrained compression tests were also performed at quasi-static strain rates.

Table 2.1. MAT_162 parameters (Source: Abrate 2011)

Density, r	ASTM C-20
Tensile modulus, E_A, E_B, E_C	AST D 3039
Poisson's ratio v_{21}, v_{31}, v_{32}	Calculated from tensile and shear modulus
Shear modulus, G_{AB}, G_{BC}, G_{CA}	ASTM D 5379/D 5379M
In-plane Tensile Strength, S_{AT}, S_{BT}	ASTM D3039
Out of plane tensile strength, S_{CT}	ASTM D 6415
Compressive strength, S_{AB}, S_{BC}, S_{CA}	ASTM D 3410/D, 3410 M-03, ASTM D 695
Fiber crush, S_{FC}	N.A.
Fiber shear, S_{FS}	N.A.
Matrix mode shear strength, S_{AB}, S_{BC}, S_{CA}	ASTM D 5379/D 5379M or ASTM D 3846
Residual compressive scale factor, S_{FFC}	N.A.
Friction angle, P_{HIC}	N.A.
Damage parameter, AM1, AM2, AM3, AM4	N.A.
Strain rate parameter, C_1, C_2, C_3, C_4	Split Hopkinson Pressure Bar
Delamination, S_DELM	N.A.
Eroding Strain, E-LIMIT	N.A.

2.2. Fabrication of E-Glass/Polyester Composite Materials

In this study, a cross-ply E-glass was selected as fiber material, and polyester was chosen as resin. The composite materials in $[0/90]_s$ fiber orientation were fabricated using Vacuum Assisted Resin Transfer Molding (VARTM) method as shown in Figure 2.1. The produced composites were used in characterization, and multi-hit impact studies in SHPB, ballistic and compression after impact tests.

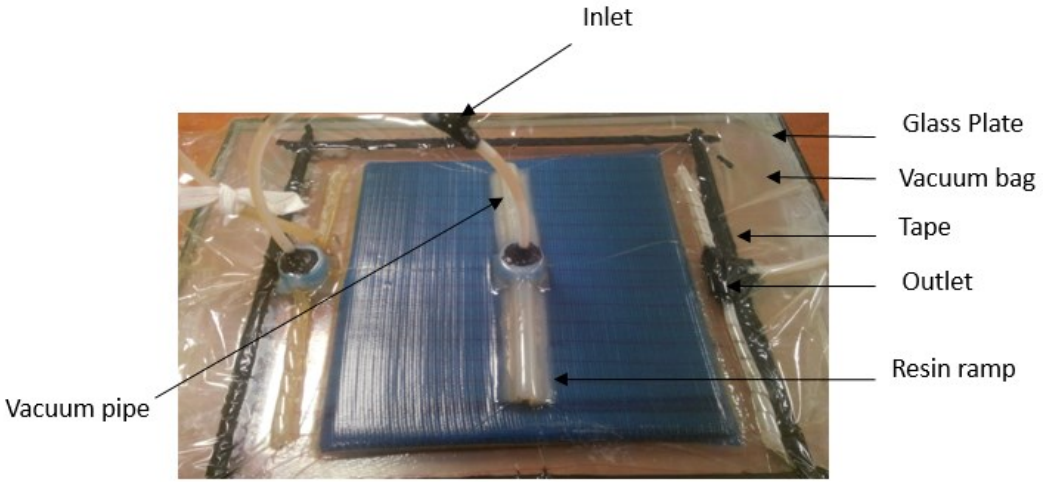

Figure 2.1. Manufacturing of composite materials using VARTM method

In this manufacturing method, the following formulation was used to calculate the required number of E-glass fiber plies for a given thickness

$$n = \frac{h\rho_f V_f}{mof} \tag{2.1}$$

In this formulation ;

- The number of fiber plies is shown as n
- The given thickness of composite laminate is shown as h
- The density of fiber material is shown as ρ_f
- Fiber volume fraction is shown as V_f
- The areal density of fiber is shown as mof

The density and areal density of E-glass fiber material are 2600 kg/m^3 and 600 g/m^2, respectively. A value of 0.6 was chosen as fiber volume fraction to fabricate composite materials.

To calculate the amount of polyester resin (Crystic PAX 703), the following formulation was used

$$m_p = (\rho_m V_m) V_p \tag{2.2}$$

In this formulation ;

- The mass of the resin is shown as m_p
- The density of the resin is shown as ρ_m
- The volume fraction of the resin is shown as V_p
- The final volume of the composite plate is shown as V_m

The density of the resin is 1200 kg/m^3 and the mass of hardener used in manufacturing the composite materials is 3 wt% of the resin.

After calculating the number of the fiber plies and the required mass of the resin for a given thickness, the composite plates were manufactured using the VARTM method. In this method, first a thin layer of wax material was applied to a glass surface. Then, fibers needed for final composite plate thickness were stacked upon the glass plate. After all the fibers were placed, they were covered with tear-off and draining tissue sequentially. Upon inserting resin ramps, vacuum bag was placed over draining tissue to provide air sealing. After the vacuum bag was sealed with sealtex, the resin was transferred into the vacuum bag using a vacuum pipe. An electrical motor was also used to pump the resin into the fibers.

2.3. Characterization of E-Glass/Polyester Composite Material

Characterization tests are conducted to determine the properties of E-glass/polyester composite materials in three principal axes through quasi-static and dynamic tests, and these tests are explained in the following sections in detail.

2.3.1. Compression Tests

The quasi-static and dynamic compression tests were conducted to investigate strain rate sensitivity of composite materials in three principal axes. The cylindrical specimens used in these compression tests were core-drilled 10 mm in diameter and 10

mm in length through three principal axes from the composite plates fabricated using the VARTM method (Figure 2.2). For the quasi-static tests, Shimadzu testing device was employed while for the dynamic tests, split-Hopkinson pressure bar test set-up was used. The steps followed in the quasi-static and dynamic tests would be explained in detail in the next sections.

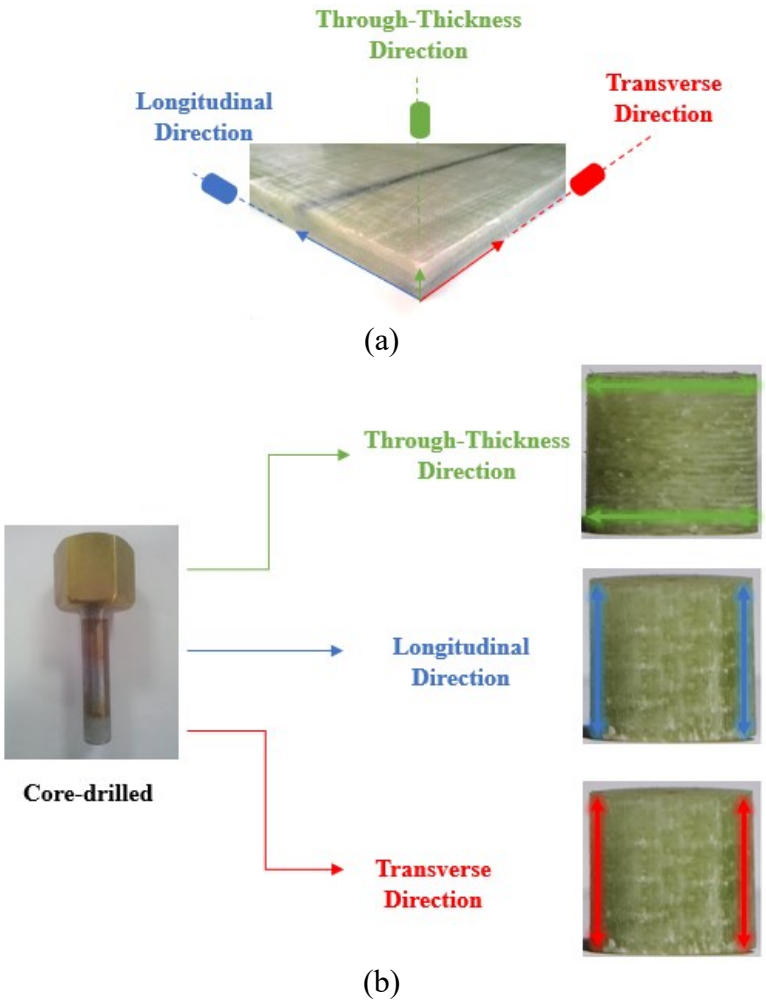

Figure 2.2. Preparation of the compression test specimens (a) the composite plate and (b) the core-drilled test specimens in three principal axis directions

2.3.1.1. Quasi-static Compression Tests

In the quasi-static tests, cylindrical composite specimens were tested in three principal axes directions at three different strain rate, namely 10^{-3}, 10^{-2} and 10^{-1}. The crosshead speeds of the testing machine corresponding these strain rates were determined using the following equation

$$V_{cr} = \dot{\varepsilon} L_o \tag{2.3}$$

where V_{cr} is the crosshead velocity of the machine, $\dot{\varepsilon}$ is the strain rate for the specimen, and L_o is the initial length of the cylindirical sample.

The deformation of composite specimens was measured using a video extensometer measuring system on the machine, and force values applied to specimens were measured from the load cell on the cross-head of the testing machine. Then, displacement and force values were transferred from the testing machine to TRAPEZIUM software program. Following tests, the stress and strain values of composites in three principal axes were calculated using the following equations

$$\sigma_{sp} = \frac{P}{A_{sp}} \tag{2.4}$$

$$\varepsilon_{sp} = \frac{\Delta L}{L_o} \tag{2.5}$$

where σ_{sp} is stress on the cylindirical specimen, P is the applied force to it, A_{sp} is the cross-sectional area of the specimen, ε_{sp} is the specimen strain, ΔL is the amount of deformation of the specimen, and L_o is the initial length of the specimen.

Ultimate compression strength and failure strain were calculated at the quasi-static strain rates. In addition, Young's modulus of the specimen in three principal axes was determined from the stress versus strain curve of the composite specimen in the low strain rates in those directions.

2.3.1.2. Dynamic Compression Tests

SHPB testing apparatus employed in dynamic compression and multi-hit impact tests, and its schematic are shown in Figure 2.3.

As shown in Figure 2.3 (b), the test set-up consists of three bars made of Vascomax C350 material, namely 700 mm striker bar, 2000 mm incident bar and 1800 mm transmitter bar.

(a)

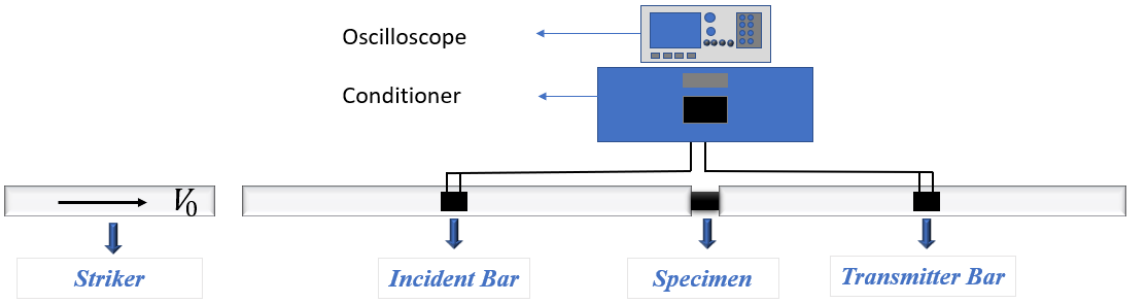

(b)

Figure 2.3. (a) SHPB test set-up and (b) its schematic

The physical properties of the bar materials are shown in Table 2.1. The cylindrical composite specimens were core-drilled in X, Y, and Z principle axis. Their dimensions were 10 in mm diameter and 10 mm in length. Also, a high-speed camera and light source were utilized to record the deformation of composite samples. Strain gages were placed on the incident and transmitter bars in an equal distance (90 mm) so as to determine strain on the bars, and the circuit type of these strain gages was Wheatstone full bridge.

Table 2.2. Mechanical properties of the Vascomax C350 bars

Physical Properties	***Values***
Density	8100 kg/m^3
Elastic Modulus	180 GPa
Poisson's Ratio	0.3

In this test device, a specimen was sandwiched between the incident bar and transmitter bar. The striker bar was accelerated by means of a gas tank, and it struck the incident bar, resulting in producing a compression pulse. This pulse propagated along the incident bar, and it was measured as an incident pulse via the strain gages placed on the incident bar. When the pulse reached the interface of the incident bar and the specimen, some part of it reflected back while the other part passed through the specimen and propagated along the transmitter bar. The reflected wave was monitored through the strain gages attached to the incident bar while the transmitter wave was recorded with the help of the strain gages attached on the transmitter bar. Then the measured waves were transferred into a signal conditioner to being conditioned. Then the voltage wave versus time curve shown on the screen of an oscilloscope was attained. A typical bar response obtained from SHPB tests can be seen in Figure 2.4 as a voltage versus time curve.

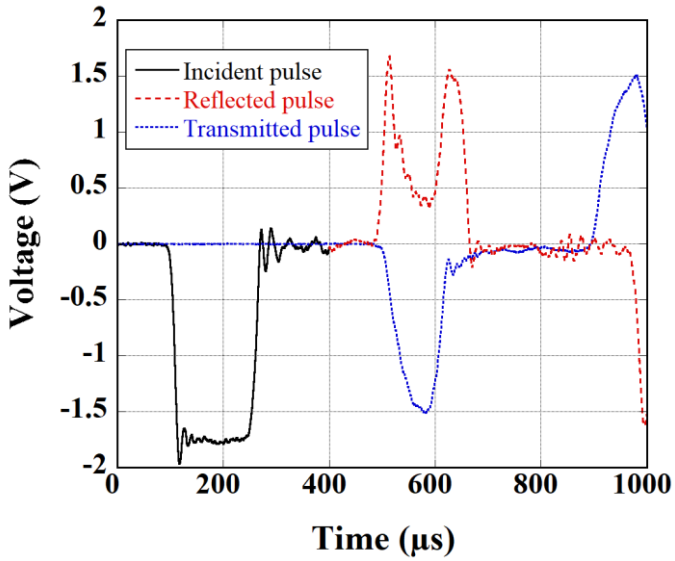

Figure 2.4. Voltage versus time curve obtained after an SHPB test of a composite specimen

After the striker bar impacts the incident bar, stress (σ_b) and strain (ε_b) occurred in the bars, and the time window (T_w) of the incident pulse can be determined using Equation 2.6-2.8 respectively.

$$\sigma_b = \frac{c_b \rho_b v_o}{2} \tag{2.6}$$

$$\varepsilon_b = \frac{\sigma_b}{E_b} \tag{2.7}$$

$$T_w = \frac{2L_{Striker}}{c_b} \tag{2.8}$$

where $L_{Striker}$ is the length of the striker bar, E_b is the Young's modulus of the bar, v_o is the striking velocity of the striker bar and c_b is the wave velocity of the striker bar.

The stress versus strain curve and stress-strain-strain rate curve of the specimen are calculated from the voltage wave versus time curve (Figure 2.4) by the following procedure.

First, the voltage values obtained from the oscilloscope are converted into strain value ($\varepsilon(t)$) as follows

$$\varepsilon(t) = \frac{2V(t)}{V_{exc}GFK_{gain}(1+v)} \tag{2.9}$$

where; V_{exc} (10 Volt) is the excitation voltage, K_{gain} (200) is the gain value which the condinitoner is set, GF (2.16) is the gage factor of the strain gage, and v (0.3) is the Poisson's ratio of the bar material.

Then using the following equations the stress, strain, and strain rate value of the specimen are calculated using the Equation 2.10-2.12 respectively.

$$\sigma_{sp}(t) = E_b \frac{A_b}{A_{sp}} \varepsilon_{trans}(t) \tag{2.10}$$

$$\varepsilon_{sp}(t) = -\frac{2c_{0_b}}{L_{0_{sp}}} \int_0^t \varepsilon_{ref}(t)\, dt \tag{2.11}$$

$$\dot{\varepsilon}_{sp} = -\frac{2c_{0_b}}{L_{0_{sp}}} \varepsilon_{ref}(t) \tag{2.12}$$

where ;

- E_b is the elastic modulus of the bar
- A_b is the surface area of the bar
- A_{sp} is the surface area of the specimen

- ε_{trans} , ε_{ref} are the transmitted and reflected strain, respectively
- $\varepsilon_{sp}(t)$ is specimen strain
- $\dot{\varepsilon}_{sp}$ is specimen strain rate
- c_{0_b} is wave velocity of the incident bar $\left(c_{0_b} = \sqrt{E_b/\rho_b}\right)$
- $L_{0_{sp}}$ is the initial length of the specimen
- $\sigma_{sp}(t)$ is specimen stress

In case of multi-hit impact tests, a cylindrical composite specimen was sandwiched between the bars. In the first impact, the striker velocity was calculated as a value at which the composite specimen did not fail. After being impacted the composite, the pre-impacted specimen was inserted into the bars again for the second impact. In the second impact, the velocity of the striker bar was determined as a value at which the damaged composite specimen failed. Besides the high-speed camera was connected to the oscilloscope using TRIG TTL IN cable to capture the deformation of composite samples at the same time.

2.3.2. In-Plane Tensile Tests

The quasi-static tension tests were performed in accordance with ASTM 3039M (ASTM International 2017). According to this test standard, the dimensions of the tension test specimen with end tabs are 2.5 mm in thickness, 25 mm in width and 250 mm in length. The dimensions of the end tabs are 1.5 mm in thickness and 50 mm in length (Figure 2.5).

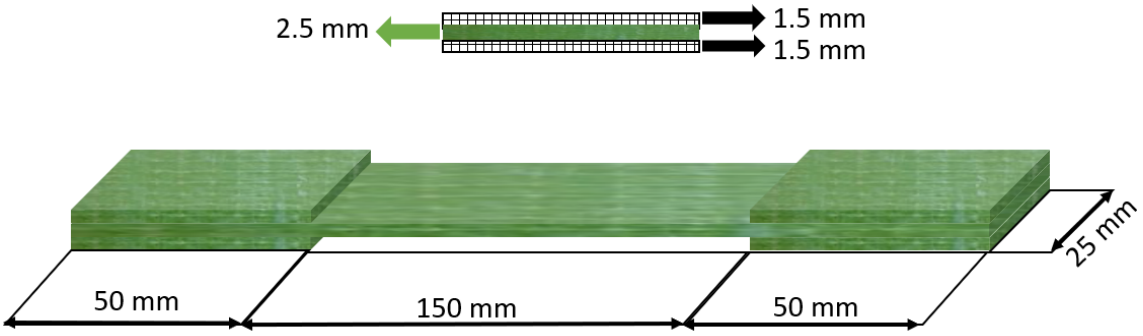

Figure 2.5. The dimension of the tension test specimen according to ASTM 3039M

A Shimadzu testing machine was used to test the specimens in the longitudinal and transverse directions at 2 mm/min cross-head velocity. The deformation of composite samples is recorded by means of the extensometer attached to the testing machine. The material of the end tabs is selected the same as that of the tension test specimen, E-glass/polyester composite. 90° tab bevel angle is used to between the test specimen and the end tabs. The end tabs are glued the E-glass/polyester composite using BISON epoxy adhesive.

The tensile strength and strain, and elastic modulus of the composite specimens in the longitudinal and transverse direction are calculated using this test method.

2.3.3. V-Notched Beam Test Method

The shear properties of composite laminate were determined according to ASTM 5379M (ASTM D5379 2012). The dimensions of the V-notched test specimen taken from this test standard are shown in Figure 2.6. Two strain gages are attached on composite specimens in ±45° directions between the notch roots as shown in Figure 2.7 to determine shear strain and shear modulus.

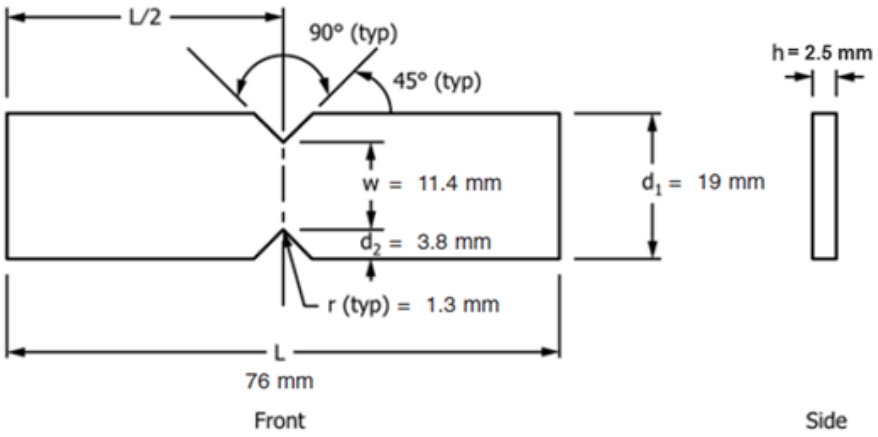

Figure 2.6. V-notched test specimen dimensions according to ASTM standards (Source: ASTM D5379 2012)

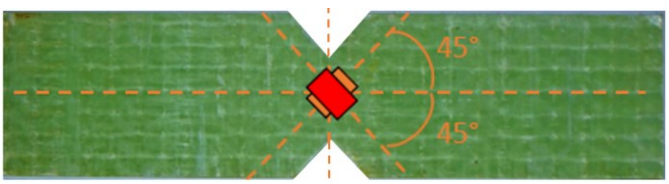

Figure 2.7. V-notched test specimen used in experiments

Shimadzu testing machine is employed for the V-notched tests, and test apparatus used are shown in Figure 2.8. This apparatus consists of two parts. One of them is fixed while the other part is moving in one direction. In this test method, after inserting the V-notched specimen into the test apparatus, force was applied to the moving part of the apparatus at 2 mm/min cross-head velocity. Then specimens failed under the shear force. The shear properties of composites were calculated using displacement and force histories obtained from the strain gages and the load cells placed on the cross-head of the machine, respectively.

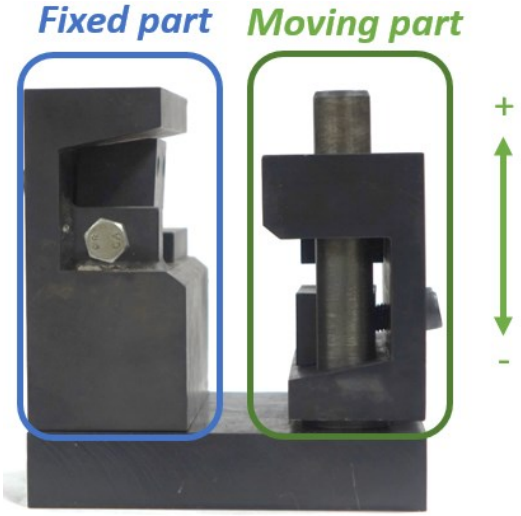

Figure 2.8. V-notched test apparatus

The shear stress of the specimen was calculated using Equation 2.13.

$$\tau = P/A \tag{2.13}$$

where τ is shear stress, P is applied force and A is the cross-sectional area of the specimens and obtained by multiplying the widht (w) and thickness (h). To determine shear strain, the followig equation was employed.

$$\gamma = |\varepsilon_{+45}| + |\varepsilon_{-45}| \tag{2.14}$$

where ε_{+45} is the +45° normal strain values and ε_{-45} is the -45° normal strain values.

2.3.4. Laterally Constrained Compression Tests

Laterally constrained test apparatuses and a cubic specimen can be seen in Figure 2.9. The test apparatuses are made of two parts, namely a laterally constrained compression jig and a steel loading pillar. Cubic composite specimens were cut from composite plates in the dimension of 12.7 mm through X, Y, and Z-axes (Yen 2012). Fiber crush strength and fiber shear strength were calculated using this test method. In this procedure, a compression load was applied to a steel loading pillar at a velocity of 1.5 mm/min, then the steel pillar compressed the laterally constrained cubic specimen in the loading direction. In such condition, the transverse compressive load caused the cubic specimen to fail at an inclined angle (θ) in the loading direction. The fiber shear strength (SFS) was determined from the ultimate strength of the cubic sample under the loading condition while the fiber crush strength (SFC) was calculated using Equation 2.15 and the inclined angle obtained from the test.

$$SFS = 0.5(SFC)\sin(2\theta) \tag{2.15}$$

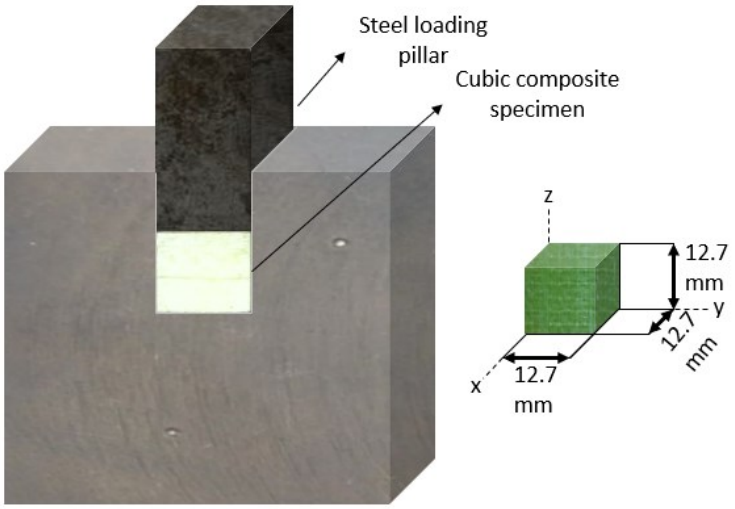

Figure 2.9. Laterally constraint test apparatus and cubic specimens

2.3.5. Elastic Constant Determination Tests

This test method was used to determine the Poisson's ratio of composite. The test apparatuses and a cubic composite specimen used in the tests are shown in Figure 2.10.

The test apparatuses consist of two rectangular steel pillars. The cubic specimen with the dimensions of 12.7 mm is sandwiched between the steel pillars. Extensometer measuring system is used to measure deformation in loading directions by attaching extensometer markers on these steel pillars. Two strain gages are also used to determine the deformation of the specimen through a loading direction and perpendicular to the loading direction. The strain gages are placed two adjacent surfaces of the sample, and one of them placed 0° position to measure contraction in length of the specimen in the force direction while the other strain gage placed 90° position to measure elongation in length of the specimen in that direction. Force is applied through the longitudinal and transverse direction, and Poisson's ratios are calculated by means of strain gages attached on the cubic samples.

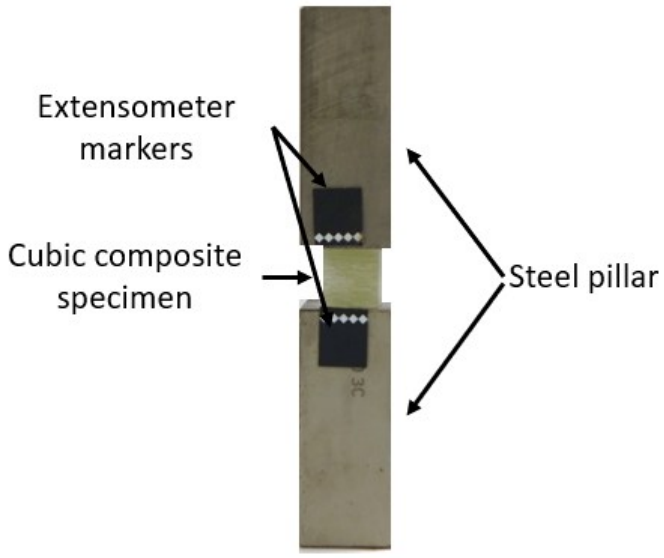

Figure 2.10. Test apparatuses and a cubic test sample for the elastic constant measuring tests

2.3.6. Projectile Impact Tests

The ballistic performance of composite laminates in 200x200x10 mm dimensions (Figure 2.11 (a)) manufactured via VARTM method is investigated using a projectile impact test set-up (Figure 2.11 (b)). The test set-up consists of a gas tank containing of pressurized air, a trigger mechanism accelerating the projectile, a polyurethane sabot helping a projectile with 30 mm in diameter and 110 g in weight to being centrally moved in a gun barrel, and a closed room being covered with iron sheets. There is a specimen holder (Figure 2.11 (c)) and laser barriers inside of the closed room. Laser barriers are used to measure the impact velocity of the projectile on composite laminates, and exit

velocity of the projectile after penetrating composite plates. To record composite plates deformation, the high-speed video camera and light source are used.

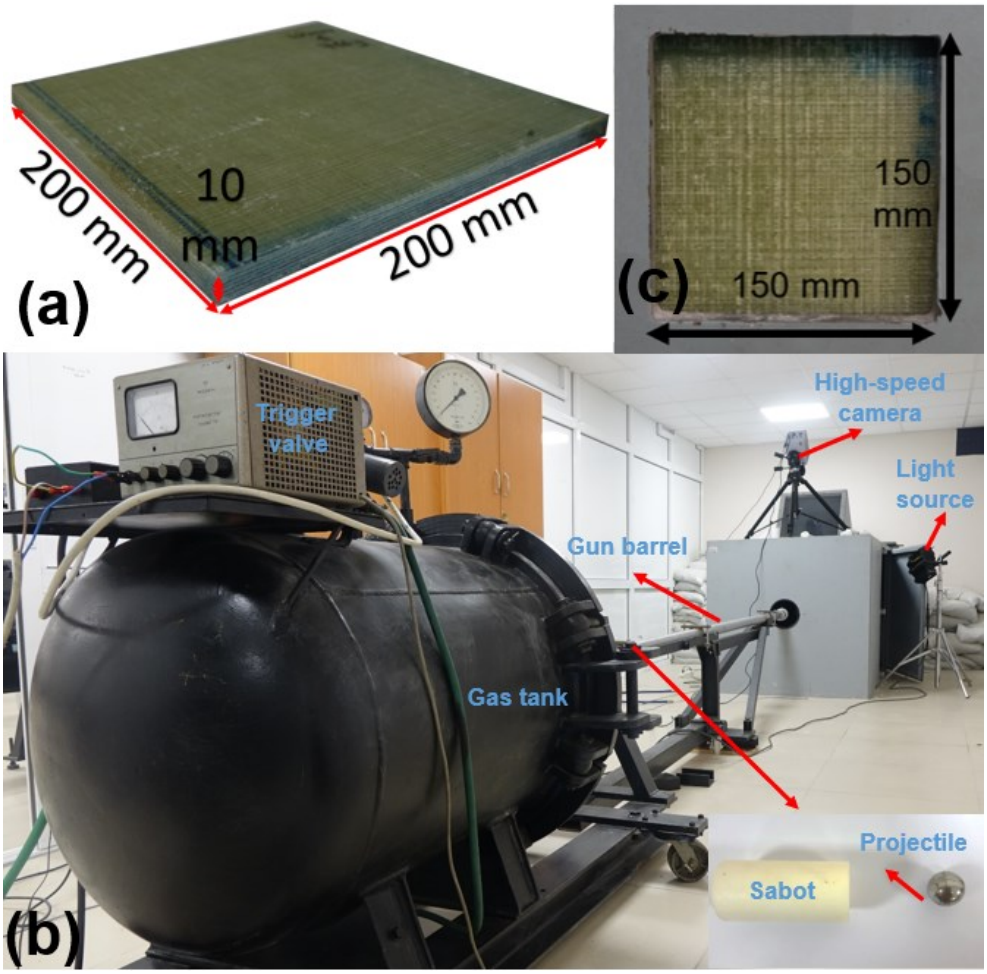

Figure 2.11. (a) Ballistic test specimen (b) the projectile test set-up (c) specimen holder

The ballistic performance and absorbed energy by composite laminates are determined after performing testing.

The test set-up is also used to calculate the residual strength of composite materials subjected to multi-hit impacts. Multi-hit impacts are obtained by changing the position of the gun barrel before being fired the projectile. Therefore, composite materials are subjected to impacts multiple times as shown in the following figure.

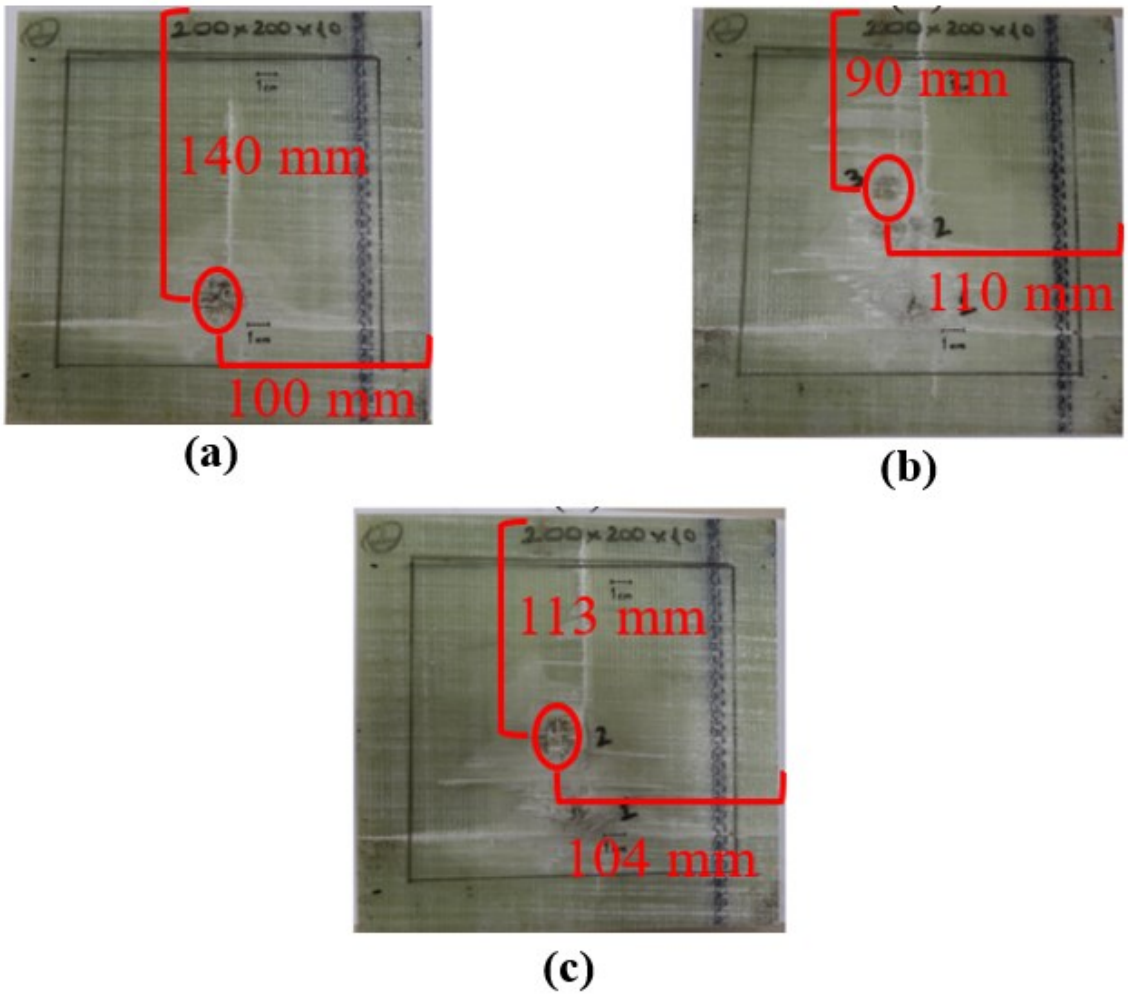

Figure 2.12. Impact positions for the multi-hit impact tests (a) the first impact, (b) the second impact and (c) the third impact

CHAPTER 3

NUMERICAL METHODOLOGY

3.1. Introduction

LS-DYNA finite element code was employed to model the tests performed on E-glass/polyester composite materials. MAT_162 composite material model in LS-DYNA was used to see damage propagation and to observe where and when damage occurred. By means of this material model, it is possible to monitor matrix damage, delamination, fiber fracture, and fiber crush. The material model parameters have first obtained by means of standard and non-standard test methods, then the results obtained from simulation with these parameters were calibrated by comparing to those obtained from experimental studies. Following the calibration steps, the multi-hit impact models for SHPB tests and projectile impact tests were formed to investigate the multi-hit impact capacity of composite materials under these impact conditions.

3.2. Despriction of Modelling and Methodology

E-glass/polyester composite materials, the top and bottom plates in quasi-static tests, bars in the SHPB, and the projectile were modeled and meshed with LS-INGRID. Quad elements were selected to mesh the composite materials and the test equipment. Then the models were transferred into LS-DYNA and opened in it as k files. In here, after material model parameters and boundary conditions were inserted into it, the material model parameters were calibrated with the quasi-static and dynamic tests. As long as the calibration process was completed, the multi-hit impact models were formed. The steps followed for the multi-hit impact models were summarized in Figure 3.1. DYNAIN file method was successfully utilized in multi-hit impact models in addition to the calibration models so as to impact on the composite materials multiple times.

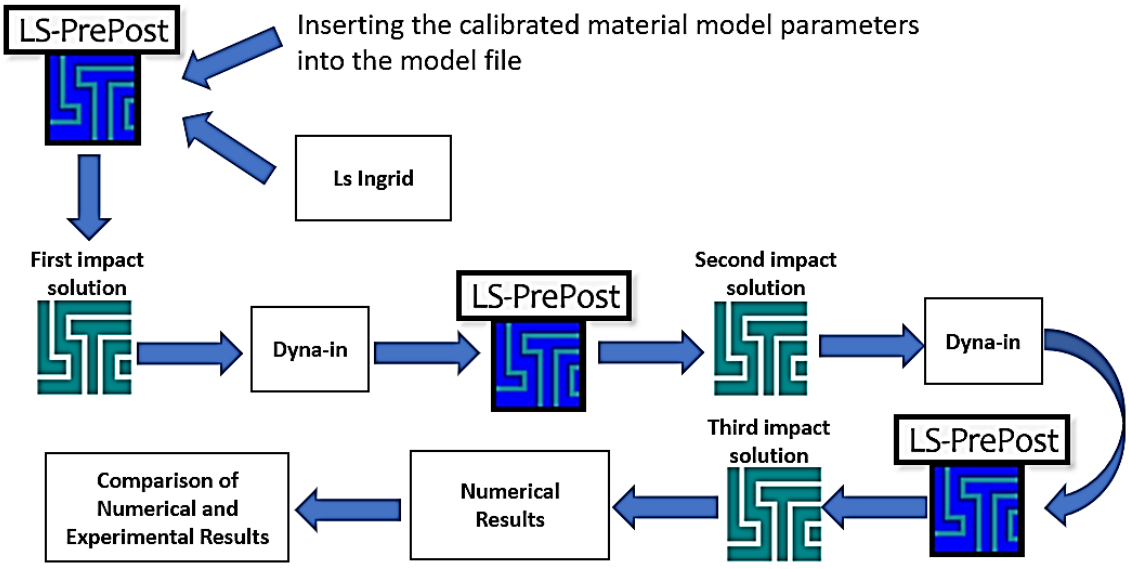

Figure 3.1. The steps followed in multi-hit impact models

3.3. MAT_162 Composite Material Model

MAT_162 material model was developed by Materials Sciences Corporation and further implemented in LS-DYNA finite element code. This material model was based on the principle of progressive failure of Hashin (Hashin 1980) and damage mechanics of Matzenmiller et al. (Matzenmiller, Lubliner, and Taylor 1995). It was used to monitor and investigate the deformation of composite laminates.

In the material model, a, b and c directions corresponding X, Y and Z principle directions are designated as the in-plane fill, in-plane warp and out-of-plane directions for fabric composites, respectively. It consists of matrix and fiber failure modes, damage model and element erosion criteria (LSTC 2015). They were explained in the following sections in detail.

3.3.1. Matrix and Fiber Failure Modes

For unidirectional composite materials, three failure criteria are utilized for the fiber fracture (tensile/shear fiber mode (f_1), compression fiber mode (f_2), crush mode (f_3)) while two failure criteria are used for the matrix failure (perpendicular matrix mode (f_4), parallel matrix mode (f_5)). To characterize the fiber damage in fabric composite materials three criteria are employed, namely fiber tensile failure (f_6, f_7), fiber

compressive failure (f_8, f_9), and fiber crush failure (f_{10}) whilst two failure criteria are employed for the matrix failure in fabric laminates, that is in-plane shear stress failure (f_{11}) and delamination mode (f_{12}). Since fabric composite materials are used in experimental and numerical studies, the failure modes for fabric laminates will be explained in the following section.

3.3.1.1. The Fill and Warp fiber Tensile/Shear Failure Modes

The fill and warp fiber tensile/shear failure modes are based on the fiber failure criteria by developed Hashin for a unidirectional composite. The quadratic interaction between the associated axial and shear stresses describe these failure modes as follows

$$f_6 = \left(\frac{\langle \sigma_a \rangle}{S_{aT}}\right)^2 + \frac{(\tau_{ab}^2 + \tau_{ca}^2)}{S_{aFS}^2} - 1 = 0 \tag{3.1}$$

$$f_7 = \left(\frac{\langle \sigma_b \rangle}{S_{bT}}\right)^2 + \frac{(\tau_{ab}^2 + \tau_{bc}^2)}{S_{bFS}^2} - 1 = 0 \tag{3.2}$$

where

- S_{aT} and S_{bT} are the axial tensile strengths in the fill and warp directions
- S_{aFS} and S_{bFS} are the layer shear strength because of fiber shear failure in the fill and warp directions.

These failure criteria are only valid in case of the associated σ_a or σ_b is positive. It is supposed that $S_{aFS} = SFS$ and $S_{bFS} = SFS * S_{bT}/S_{aT}$.

3.3.1.2. Compressive Failure in The Fill and The Warp Directions

In case of σ_a or σ_b is compressive, the maximum stress criterion describes the in-plane compressive failure in the fill and warp direction as follows

$$f_8 = \left(\frac{\langle \sigma_a' \rangle}{S_{aC}}\right)^2 - 1 = 0\,, \qquad \sigma_a' = -\sigma_a + \langle -\sigma_c \rangle \tag{3.3}$$

$$f_9 = \left(\frac{\langle \sigma_b' \rangle}{S_{bC}}\right)^2 - 1 = 0\,, \qquad \sigma_b' = -\sigma_b + \langle -\sigma_c \rangle \tag{3.4}$$

where S_{aC} and S_{bC} are the axial compressive strengths in the fill and warp directions. The crush failure of the fabric composites subjected to compressive pressure (hydrostatic pressure (p)) is defined as follows

$$f_{10} = \left(\frac{\langle p \rangle}{S_{FC}}\right)^2 - 1 = 0\,, \qquad p = \frac{\sigma_a + \sigma_b + \sigma_c}{3} \tag{3.5}$$

The S_{FC} is the layer strength related to the fiber crush failure.

3.3.1.3. In-Plane Shear Stress Failure

Failure can occur in plain weave fiber under in-plane shear stress before the fiber failure is taken place. The in-plane matrix failure mode is defined as

$$f_{11} = \left(\frac{\tau_{ab}}{S_{ab}}\right)^2 - 1 = 0 \tag{3.6}$$

The layer shear strength is designated as S_{ab}. It depends on matrix shear failure.

3.3.1.4. Delamination Failure

This failure mode occurs in case of a matrix failure is mainly taken place. The matrix failure criterion in through-thickness direction is defined as follows

$$f_{12} = \left\{\left(\frac{\langle\sigma_c\rangle}{S_{cT}}\right)^2 + \left(\frac{\tau_{bc}}{S_{bc}}\right)^2 + \left(\frac{\tau_{ca}}{S_{ca}}\right)^2\right\} - 1 = 0 \tag{3.7}$$

where S_{cT} is the through thickness tensile strength, and S_{bc}, and S_{ca} are the shear strengths believed to be influenced by the compressive normal stress (σ_c) and the coulomb friction angle (φ). The relation between the shear stresses, the compressive normal stress and the coulomb friction angle is as follows

$$\left\{\frac{S_{ca}}{S_{bc}}\right\} = \left\{\frac{S_{ca}^{(0)}}{S_{bc}^{(0)}}\right\} + \tan(\varphi)\langle-\sigma_c\rangle \tag{3.8}$$

3.3.2. Damage Model

Damage functions are obtained from the failure criteria of fiber and matrix failure modes without the Poisson's effect. Elastic moduli reduction can be defined with the relevant damage parameters $\bar{\omega}_i$ as follows

$$E_i' = (1 - \bar{\omega}_i)E_i$$

$$\bar{\omega}_i = 1 - \exp(-r_i^{m_i}/m_i) \qquad r_i \geq 0 \quad i = 1, \dots, 6$$

where E_i are the initial elastic moduli, E_i' are the reduced elastic moduli, r_i are the damage thresholds for fiber damage, matrix damage and delamination. They are calculated from the relevant damage functions. m_i are material damage parameters. To predict the overall nonlinear elastic response of a lamina containing first the initial hardening and then softening following the ultimate strengths, the damage function is examined. The aforamentioned damage paremeters made of fiber damage in the X direction (m_1), fiber damage in the Y direction (m_2), fiber crush and punch shear damage (m_3), and matrix failure and delamination damage (m_4).

3.3.3. Effect of Strain Rate on the Strength and Modulus

The effect of strain rate on the strength properties of the composite laminates can be explained as follows

$$\{S_{RT}\} = \{S_0\}\left(1 + C_{rate1} \ln \frac{\{\dot{\bar{\varepsilon}}\}}{\dot{\varepsilon}_0}\right) \tag{3.9}$$

$$\{S_{RT}\} = \begin{Bmatrix} S_{aT} \\ S_{aC} \\ S_{bT} \\ S_{bC} \\ S_{FC} \\ S_{FS} \end{Bmatrix} \text{ and } \{\dot{\bar{\varepsilon}}\} = \begin{Bmatrix} |\dot{\varepsilon}_a| \\ |\dot{\varepsilon}_a| \\ |\dot{\varepsilon}_b| \\ |\dot{\varepsilon}_b| \\ |\dot{\varepsilon}_c| \\ (\dot{\varepsilon}_{ca}^2 + \dot{\varepsilon}_{bc}^2)^{1/2} \end{Bmatrix} \tag{3.10}$$

where $\{S_{RT}\}$ is the strength values of the fiber failure modes, $\{S_0\}$ are the strength values of $\{S_{RT}\}$ at the reference strain-rate $\dot{\varepsilon}_0$, and C_{rate1} is the strain rate-constants for strength propeties.

The effect of strain rate and damage parameter on the elastic properties of the composite laminates can be explained as follows

$$\{E_{RT}\} = \{E_0\}\left(1 + C_{rate} \ln \frac{\{\dot{\bar{\varepsilon}}\}}{\dot{\varepsilon}_0}\right) \tag{3.11}$$

$$\{E_{RT}\} = \begin{Bmatrix} E_a \\ E_b \\ E_c \\ G_{ab} \\ G_{bc} \\ G_{ca} \end{Bmatrix}, \{\dot{\bar{\varepsilon}}\} = \begin{Bmatrix} |\dot{\varepsilon}_a| \\ |\dot{\varepsilon}_b| \\ |\dot{\varepsilon}_c| \\ |\dot{\varepsilon}_{ab}| \\ |\dot{\varepsilon}_{bc}| \\ |\dot{\varepsilon}_{ca}| \end{Bmatrix} \text{ and } \{C_{rate}\} = \begin{Bmatrix} C_{rate2} \\ C_{rate2} \\ C_{rate4} \\ C_{rate3} \\ C_{rate3} \\ C_{rate3} \end{Bmatrix} \tag{3.12}$$

where $\{E_{RT}\}$ is the elastic moduli, $\{E_0\}$ are the modulus values of $\{E_{RT}\}$ at the reference strain rate $\dot{\varepsilon}_0$, C_{rate2} is the strain rate constant for elastic moduli in the X direction, C_{rate3} is the srain rate constant for shear moduli and C_{rate4} is the strain rate constant for elastic moduli in the Z direction.

3.3.4. Element Erosion

Since the eroded elements cause to instabilities and unnecessary computational time, element erosion criteria have a significant effect on the verification of numerical results with the experimental results. Eroding of a failed element can be taken place in the following ways ;

- If the tensile strains of in-plane directions exceed E_LIMT value
- If compressive relative volume in a failed element is smaller than ECRSH
- If tensile relative volume in a failed element is greater than EEXPN.

3.4. Modeling of Experimental Tests in LS-DYNA

To calibrate numerical models of quasi-static and dynamic tests with experimental studies and validate numerical multi-hit impact results with experimental ones, these numerical models have been performed in Ls-dyna finite element code.

3.4.1. Modeling of Quasi-static Compression Tests

Numerical models of quasi-static compression tests for cylindrical composite samples in transverse and through-thickness directions are depicted in Figure 3.2. The numerical models encompasses cylindrical composite specimens in transverse and torugh-thickness directions, the top plate and bottom plate, which modeled and meshed in LS-Ingrid. Then the numerical models with meshed were transferred into the LS-DYNA. The dimensions of the top and bottom plate are 15 mm in diameter and 5 mm in length. The cylindrical composite specimens are 10 mm in diameter and 10 mm in length for both transverse and through-thickness direction. The optimum mesh element size was selected as 0.454x0.454x0.454 mm for composite specimens transverse direction and 0.35x0.35x0.22 mm for specimens in through-thickness direction. The bottom plate was completely constraint in three translational and rotational movements while the top plate was freely moved in the Z direction. The velocity of the top plate was set to 10^{-4} m/s in the negative Z direction using PRESCRIBED_MOTION_SET in Boundary keyword. The layer numbers of cylindrical composite materials in the transverse and through-

thickness direction were 22. Also, 0° and 90° fiber orientation were assigned to the composite layers using the BETA option in MAT_162 material model. For both specimens in transverse and through-thickness directions, ERODING_SINGLE_SURAFACE was chosen for contact condition between the plates and composite specimens, and between specimen layers. 0.3 and 0.2 were utilized for the static and dynamic friction of coefficient in ERODING_SINGLE_SURAFACE contact.

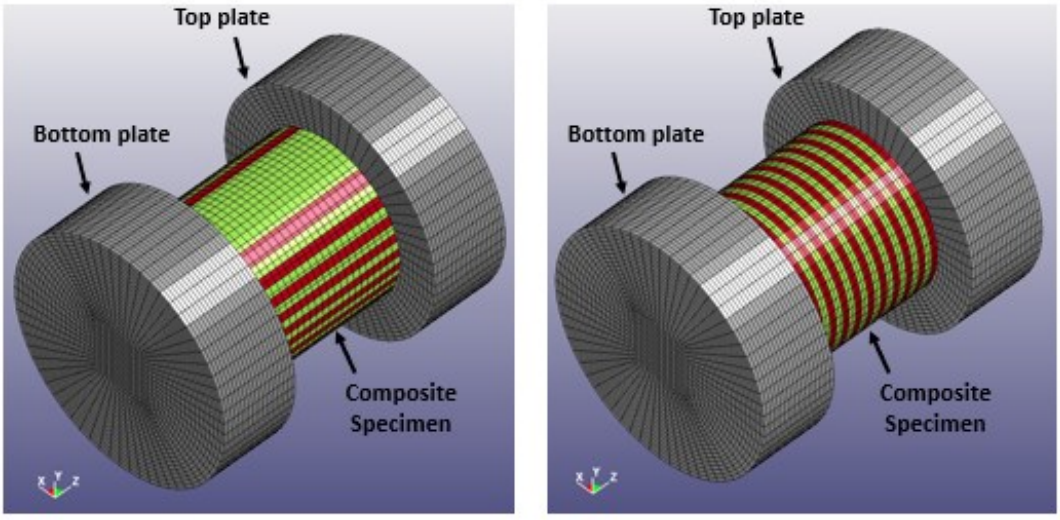

(a) (b)

Figure 3.2. The numerical quasi-static compression model for the specimen (a) in the transverse and (b) in the through-thickness direction

3.4.2. Modeling of SHPB Test Set-up

The SHPB model consisted of cylindrical specimens in transverse and through-thickness direction and bars (Figure 3.3). The bars and specimens had the same dimensions as those used in the experimental studies.

The numerical models of SHPB were formed without the striker bar. The incident stress pulse obtained from experimental studies was defined in numerical models using CURVE option in DEFINE curve. Then, this incident stress pulse was applied to the top surface of the incident bar using SEGMENT_SET option in LOAD keyword. Therefore, it was provided that impact velocity in numerical models was the same as in the experimental study. ERODING_SINGLE_SURFACE contact was assigned between the bars and specimens, and between specimen layers. The static and dynamic coefficient in contact option was taken as 0.3 and 0.2, which were the same coefficients as in quasi-

static compression models. Impact time was determined as 1000 μs, which was the same impact time as in experimental studies. It was defined in the numerical models using TERMINATION option in CONTROL keyword.

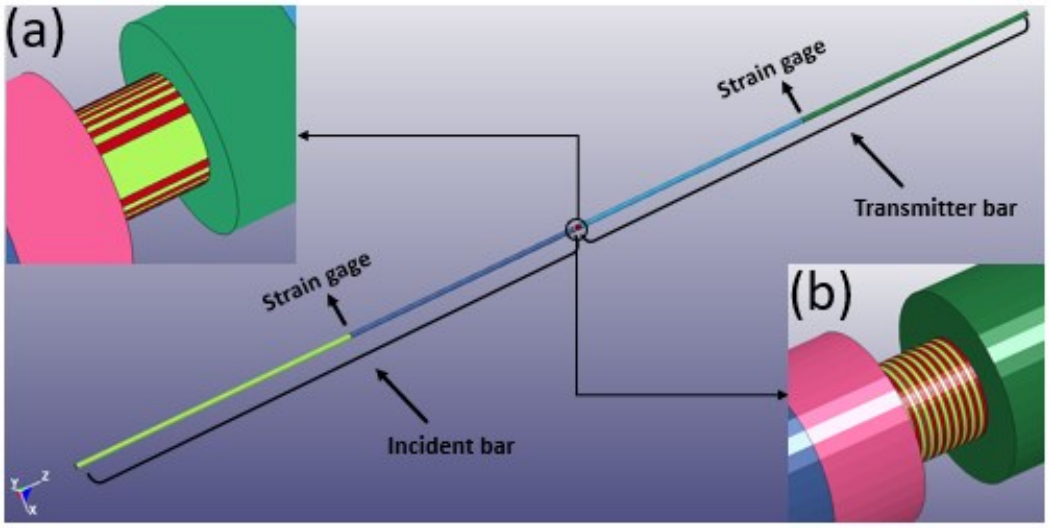

Figure 3.3. The SHPB model for (a) in-plane direction and (b) through-thickness direction specimens

In numerical models of multi-hit impacts, SPRINGBACK_LSDYNA option in INTERFACE keyword is utilized in order to impact on cylindirical composite specimens multiple times. This method is called as DYNAIN file method. The method allows to transfer the damage occurred in the first impact to the subsequent loading. In the card of this option, the specimen is defined in the part set section, and the number of additional histories variables was chosen as 36. After the intact cylindrical composite specimen is impacted, the pre-damaged specimen is taken from the file where the simulation is saved, and it is called in this file as DYNAIN. After that, the DYNAIN file is opened with the LS-DYNA, and it is employed as input for the second impact model. The steps followed during multiple impacts are summarized earlier in Figure 3.1.

3.4.3. Modeling of Projectile Impact Tests

Projectile impact test model is illustrated in Figure 3.4. The total number of solid elements is 152896 in the model. It consists of composite laminates and the hardened steel sphere projectile. The composite laminates are 200 mm in length, in 200 mm in width and 10 mm in thickness while the hardened steel sphere projectile is in 30 mm

diameter. JOHSON_COOK material model is used for the projectile in the numerical model, and the velocity of the projectile is set to 130 m/s using VELOCITY_GENERATION option in INITIAL keyword.

To apply boundary conditions on the composites, node sets are first created on the top surface and bottom surface of the laminates using SET_NODE option in SET DATA keyword. Then, they are fully constraint in the three translational and rotational movements as shown in Figure 3.4 (a). ERODING_SINGLE_SURFACE contact is used between the projectile and composite laminates, and between the layers of the composite laminates.

Multi-hit projectile impact models are shown in Figure 3.4 (b), (c) and (d) for the first, second and third impact model events, respectively. These multiple impact models are formed the same as in experimental studies. It means that for each impact the performed experimental tests are modeled in numerical studies. Shot locations are determined from the surface of composites for numerical models. The projectile is placed the same shot locations. SPRING_BACK option is used to model multiple impacts as previously mentioned.

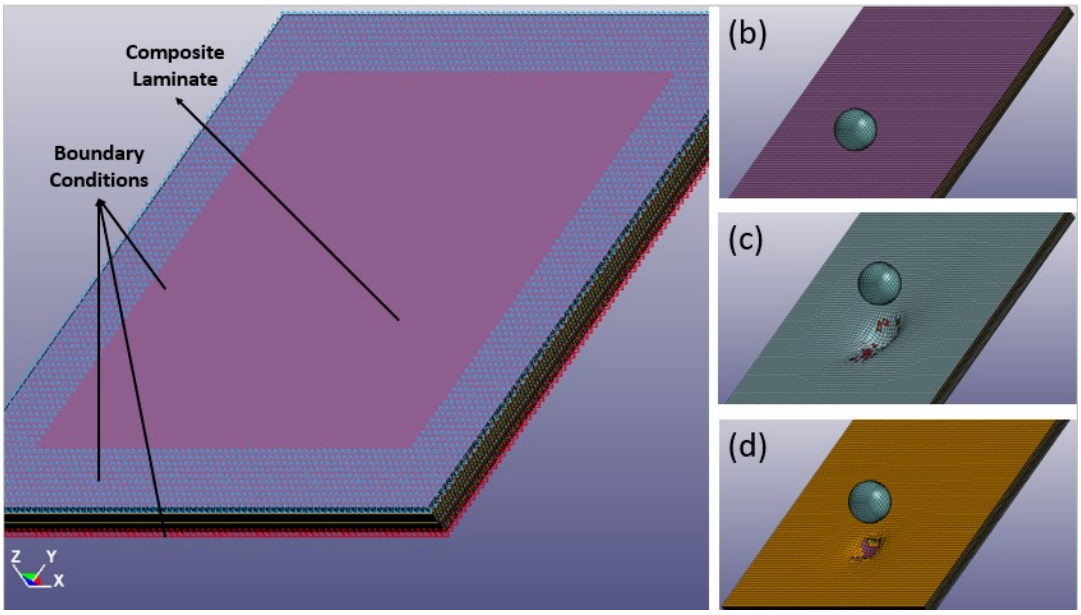

Figure 3.4. (a) Boundary conditions for the projectile impact test model, the projectile impact model (b) with the intact specimen, (c) with the damaged specimen (d) with the specimen impacted two times

To validate the accuracy of the results obtained from numerical multi-hit impact models formed in DYNAIN method, another numerical multi-hit impact model is

simulated utilizing the conventional method (Figure 3.5). In this method, a certain time interval between the projectiles is employed to create multi-hit impact on composite materials (Haque, Harrington, and Gillespie 2012b; Kong, Jiang, and Liu 2012; Prakash, Srinivasan, and Rao 2017). In this study, 1000 µs is selected as a time interval between the projectiles. The distance between the projectile and the composite is calculated by multiplying impact velocity (130 m/s) with the change in time for each projectile. The position of the projectiles is selected the same as that of the projectiles obtained from experimental ones. By using the birth and death time in ERODING_SINGLE_SURFACE contact option, the projectile is removed from the model after its kinetic energy is completely transferred to the composite.

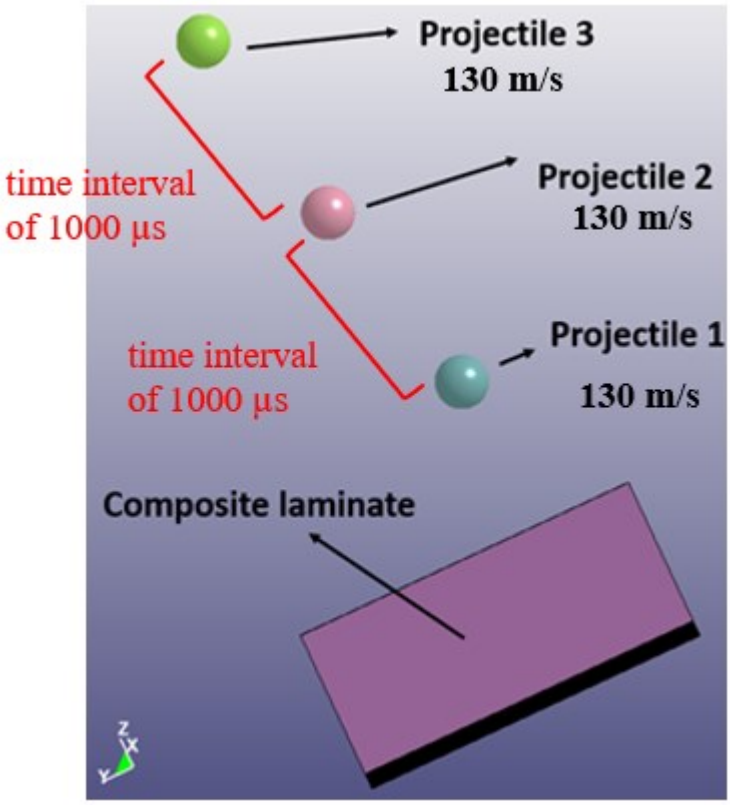

Figure 3.5. Numerical ballistic test model formed by the conventional method

CHAPTER 4

EXPERIMENTAL AND NUMERICAL RESULTS

4.1. Introduction

In this section, experimental results obtained from quasi-static compression tests, dynamic compression tests, tension tests, v-notched tests, and projectile impact tests were explained. Moreover, the required parameters for MAT_162 were calculated from the tests performed, and they were calibrated with experimental results. For the calibration of numerical models, numerical quasi-static and SHPB test models were formed while multi-hit impact models were formed for SHPB and projectile impact tests following the parameters validated.

4.2. Experimental and Numerical Test Results of E-Glass/Polyester Composite Materials

Numerical and experimental calibration and multi-hit test results were explained in the following sections. First, numerical model parameters were obtained through quasi-static and high strain rate tests, then calibrated. After that, numerical and experimental multi-hit impact test results were compared.

4.2.1. Quasi-static and Dynamic Compression Test Results

Strain rate sensitivities of E-Glass/Polyester composite materials in three principal axes are investigated to determine MAT_162 parameters related to rate dependency. For this purpose, characterization tests are performed at quasi-static strain rates (10^{-3}, 10^{-2} and 10^{-1} s^{-1}) and dynamic strain rates (300-1100 s^{-1}). Stress versus strain results at different strain rates for three different directions are illustrated in Figure 4.1 and Figure 4.2. In these figures, it can be clearly seen that failure stresses and strains, and elastic moduli increase with increasing strain rates except the failure strains of specimens in the longitudinal and through-thickness directions at high strain rates. Also, it is seen in Figure

4.1 (a-b) that the failure stresses and strains of composites in the transverse direction are more rate sensitive rather than those in the longitudinal direction at high strain rates. When comparing the failure stresses and strains in both directions, they show very much similar rate sensitivity at low strain rates. Moreover, the influence of strain rates on the elastic moduli and failure strength among three directions is more pronounced in the through-thickness direction than the other directions as seen in Figure 4.2.

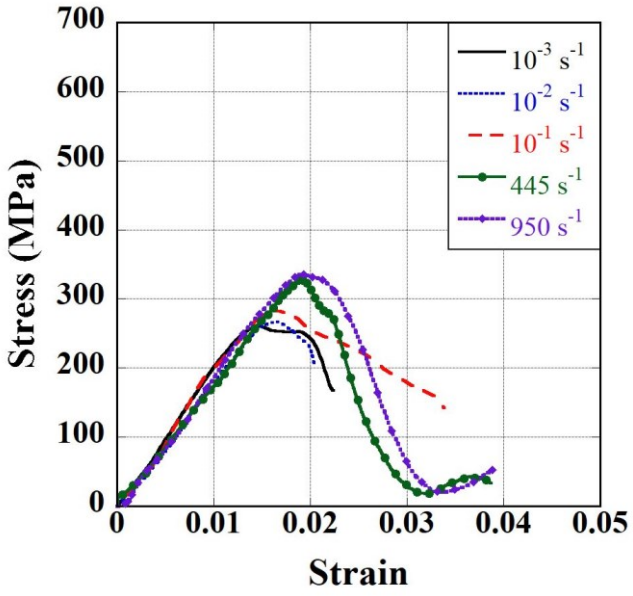

(a)

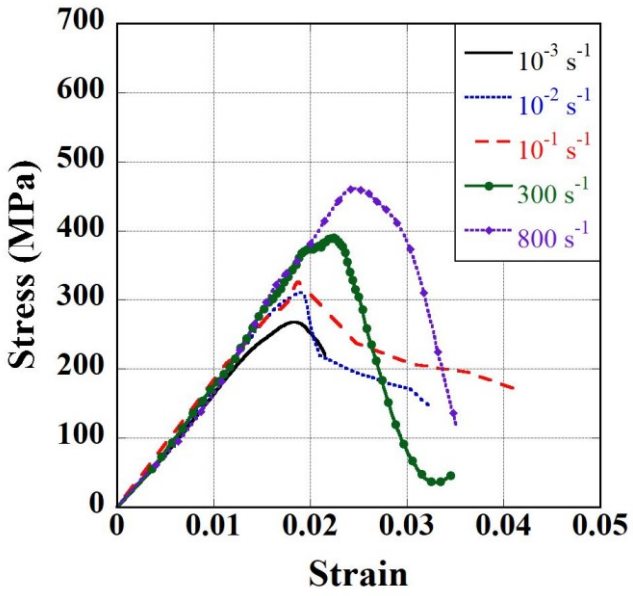

(b)

Figure 4.1. Stress versus strain curves of the specimens in (a) longitudinal and (b) transverse directions

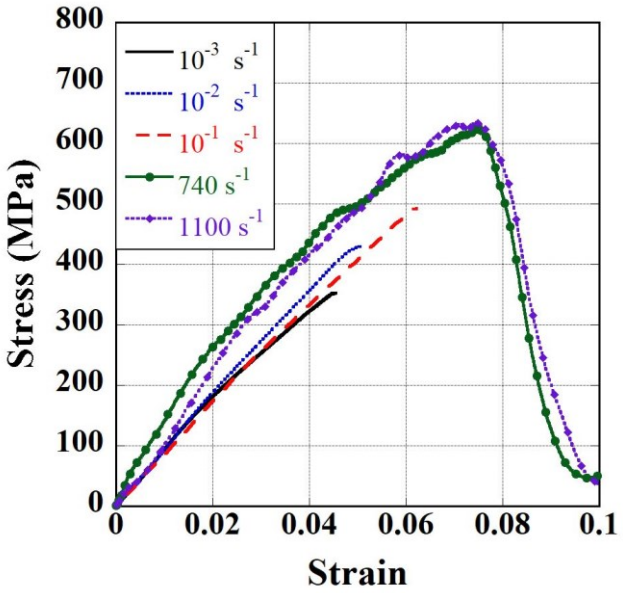

Figure 4.2. Stress versus strain curves of the specimen in the through-thickness direction at quasi-static and high strain rates

In the results of longitudinal specimens, the average strength increases from 289 to 354 MPa with increasing the strain rate from 10^{-3} to 950 s^{-1}. The average elastic modulus increases from 19.208 to 20.28 GPa at the same strain rate ranges. In the results of transvers specimens, the average strength and modulus are 290 MPa and 20.51 GPa at 10^{-3} strain rate while they are 435 MPa and 21.39 at 800 s^{-1}, respectively. It is clearly seen that in the transverse direction, the average strength and moduli increase with increasing strain rates. Besides, the average strength of specimens in the through-thickness direction increases from 390.52 to 642.69 MPa while the elastic modulus increases from 7.8 to 9.9 GPa as strain rate increases from 10^{-3} to 1100 s^{-1}. These figures indicate that the lowest strength is in longitudinal directions while the highest strength is in through-thickness directions.

The experimental and numerical compression test results of composite samples in transverse and through-thickness directions at quasi-static and high strain rates are presented in Figure 4.3 and Figure 4.4. For the composite specimen tested experimentally in the transverse direction (Figure 4.3), the value of failure stress is nearly 325 MPa at the quasi-static strain rate and 375 MPa at the high strain rate. The corresponding failure strains are 0.0175 and 0.02, respectively. For through-thickness specimens (Figure 4.4), the value of stress is 483 MPa at the quasi-static strain rate and 625 MPa at the high strain rate with the corresponding failure strain of 0.06 and 0.07, respectively. For the composite specimen tested numerically in the transverse direction, the failure stress is nearly 300

MPa at the quasi-static strain rate and 360 MPa at the high strain rate with the corresponding failure strain of 0.018 and 0.019. For composites in through-thickness directions, the failure stress is 475 MPa at quasi-static strain rates. The corresponding failure strain is 0.05. The failure stress is 606 MPa at high strain rates with corresponding strain of 0.066.

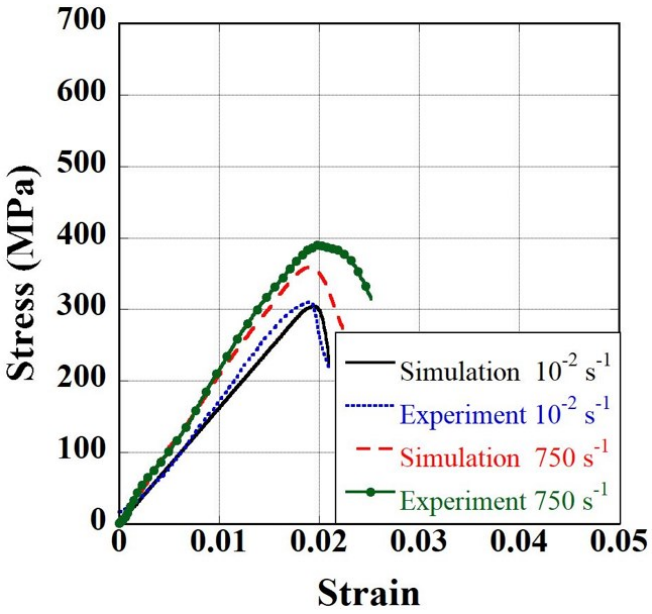

Figure 4.3. The experimental and numerical compression test results in the transverse direction

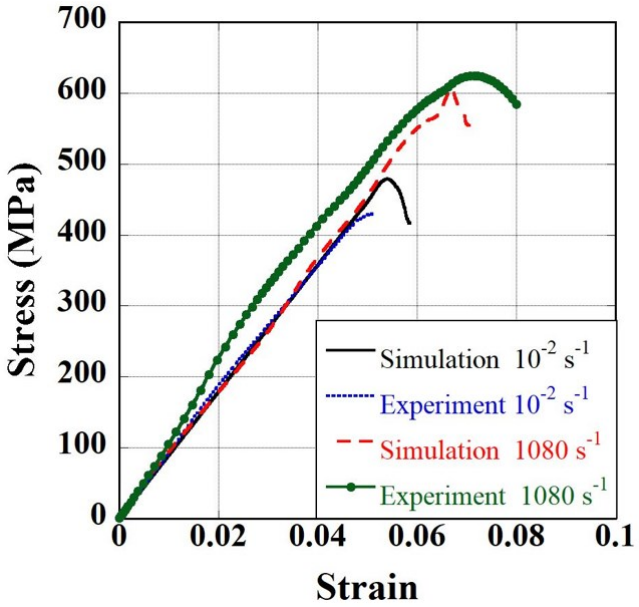

Figure 4.4. The experimental and numerical compression test results in the through-thickness direction

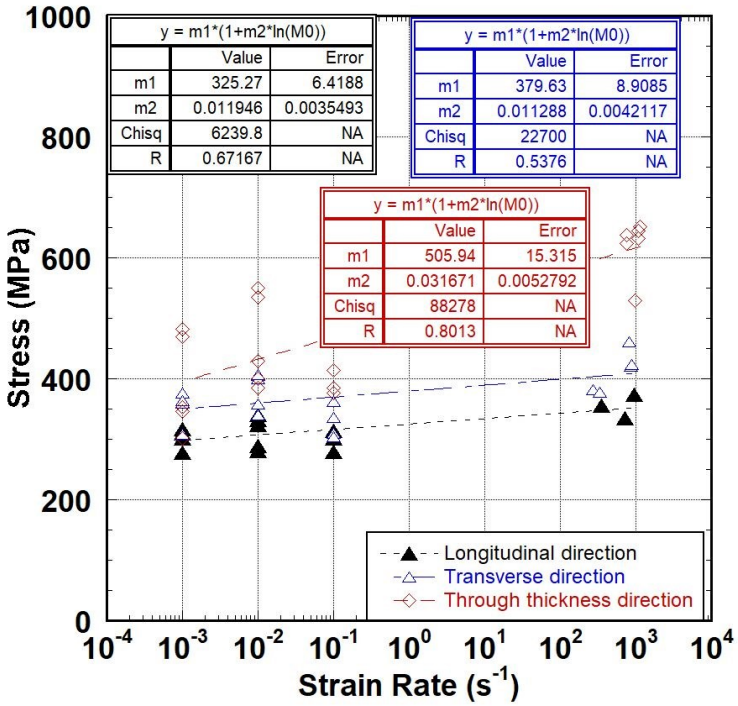

Figure 4.5. Strain rate sensitivity of the failure stresses in three different directions

The influence of strain rates on the failure stress and elastic modulus of composites in three different directions is summarized as shown in Figure 4.5 and in Figure 4.6, respectively. For three different directions, stress values obtained from three principal axes shown in the stress versus strain rate plot are fitted with Equation 3.9 while elastic moduli for these directions shown in the elastic modulus versus strain rate plot are fitted with Equation 3.11. The value of the stress and elastic modulus corresponding 1 s^{-1} (m1 values in tables) are selected as the compressive strength and elastic modulus in these directions. The compressive strengths are calculated as 325.27 MPa for the longitudinal direction, 379.63 MPa for the transverse direction and 505.94 MPa for the through-thickness direction. The strength values in longitudinal and transverse directions are assumed to be the same due to the fact that the fibers are almost biaxial. Also, elastic modulus in these directions are calculated as 20.2 GPa while the elastic modulus in the through thickness direction is found as 8.7 GPa. Moreover, m2 values in these tables represent C_{rate} in Equation 3.9 and 3.11. Using these m2 values (0.012 for the longitudinal direction, 0.011 for transverse direction and 0.032 for through-thickness direction), the average value of C_{rate1} is determined as 0.0183. In Figure 4.6, the value of C_{rate2} is determined from the elastic modulus versus strain rate graph fitted with Equation 3.11 by taking the average of m2 values of longitudinal and transverse directions (0.00094 for the longitudinal direction and 0.0027 for transverse direction), and it is

calculated as 0.001846. In the same graph, the value of C_{rate4} is selected as 0.0163, which is the value of m2 in through thickness direction.

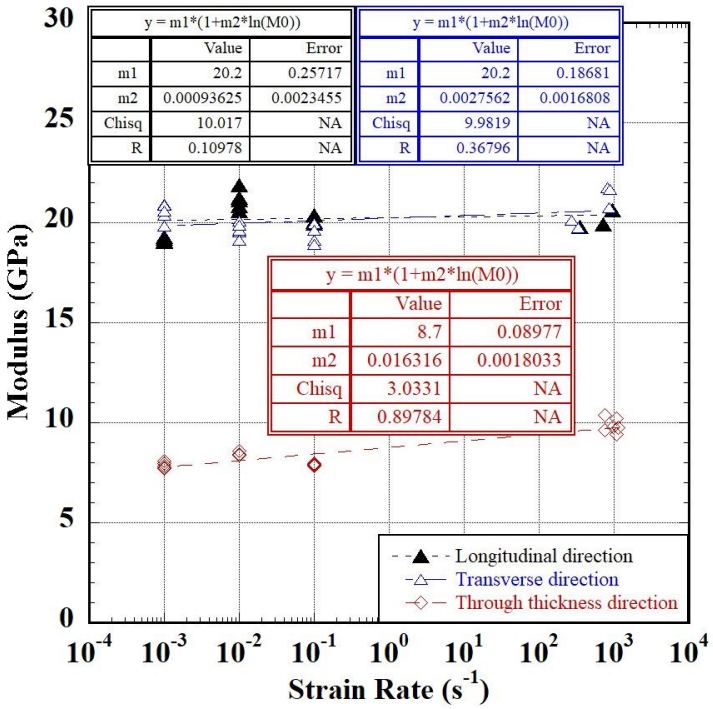

Figure 4.6. Strain rate sensitivity of the elastic moduli in three different directions

Experimentally and numerically failed transverse specimens at quasi-static strain rates and experimentally failed specimen at high strain rate are shown in Figure 4.7 (a-c). Due to low interfacial strength between the fiber and the resin, delamination was found to be a major failure mechanism between fiber and the resin in the transverse direction. With increasing in strain rate, the specimens split along the loading direction. The deformed specimens along transverse directions are shown in Figure 4.7 (a) for experimental (10^{-2} s^{-1}), in Figure 4.7(b) for numerical (10^{-2} s^{-1}) and Figure 4.7 (c) for experimental (750 s^{-1}). In the through-thickness direction, a crack occurs at the top side of the specimen in contact with the top plate. This crack caused the matrix and fiber fracture in that direction, as shown in Figure 4.8 (a-c).

Delamination contours of the numerically damaged specimen in transverse and through-thickness directions at quasi-static strain rate can be seen in Figure 4.7 (b) and in Figure 4.8 (b), respectively. For the specimen in the transverse direction, the delamination was the major failure mode between the fiber and resin. In the through-thickness direction, the crack occurs the at the top part of the specimen (in contact with the top plate). It causes the composite to be divided into two parts, and the damage extends

the top side of the specimen. Therefore, the matrix and fiber fractrure are observed for the composite. At the bottom side of the specimen does not have any significant damage when comparing the top side of it.

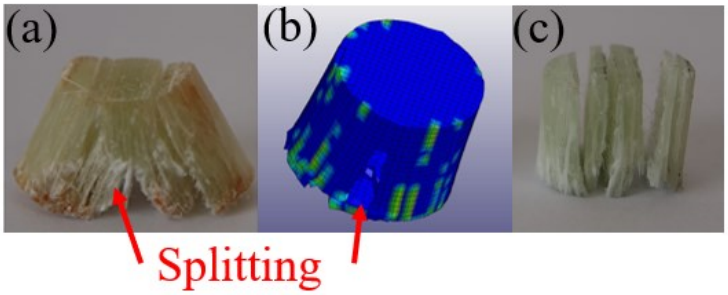

Figure 4.7. The failed specimen in the transverse direction (a) experimental (10^{-2} s^{-1}), (b) numerical (10^{-2} s^{-1}) and (c) experimental (750 s^{-1})

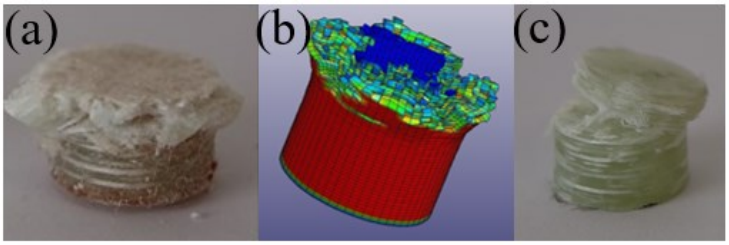

Figure 4.8. The failed specimen in the through-thickness direction (a) experimental (10^{-2} s^{-1}), (b) numerical (10^{-2} s^{-1}) and (c) experimental (1080 s^{-1})

4.2.2. Tension Test Results

The tensile stress versus strain was calculated for longitudinal and transverse directions according to ASTM 3039M, and the results are shown in Figure 4.9. The stress versus strain curves of specimens in these directions show almost linear behavior until the failure stresses and strains. After the failure strain values, the stress values suddenly drop to zero, and the specimens fail. In the longitudinal direction, the failure stresses and elastic moduli are 383 MPa and 18.14 GPa for Test 1, 368 MPa and 18.19 GPa for Test 2, and 365 MPa and 17.31 GPa for Test 3. The corresponding failure strains are 0.019, 0.02 and 0.022, respectively. In the transverse direction, the failure stresses and elastic moduli are 366.6 MPa and 19.7 GPa for Test 1, 359.7 MPa and 18.89 GPa for Test 2, 365 MPa and 20.25 GPa for Test 3, and 405 MPa and 21.3 GPa for Test 4. The corresponding strains are 0.019, 0.018, 0.016 and 0.019, respectively. In the longitudinal direction, the

average value of the failure stresses, strains and elastic moduli in the longitudinal direction are 372 MPa, 0.02 and 17.8 GPa, respectively. In the transverse direction, the average of the failure stress, strain, and elastic moduli are calculated as 374.08 MPa, 0.018 and 20.04 GPa, respectively. The results show that the mechanical properties in the longitudinal direction show very much similar properties to those of the transverse direction.

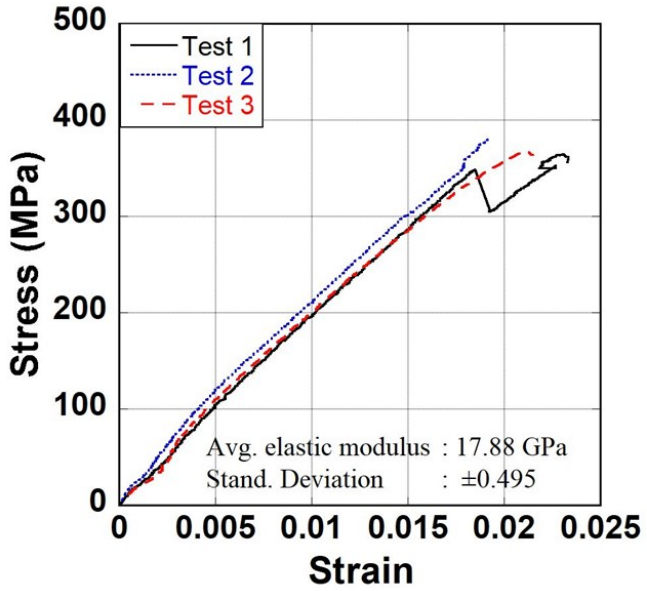

(a)

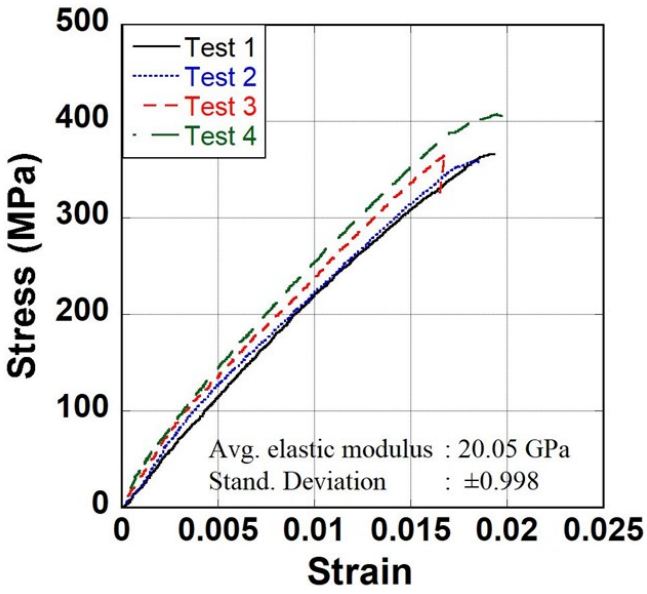

(b)

Figure 4.9. Tensile stress versus strain curves of composites specimens in (a) longitudinal and (b) transverse directions

The failed tensile test specimens are shown in Figure 4.10 (a) for the longitudinal direction and in Figure 4.10 (b) for the transverse direction. Fiber pull-out, delamination and fiber fracture are seen to be the main failure mode in these directions.

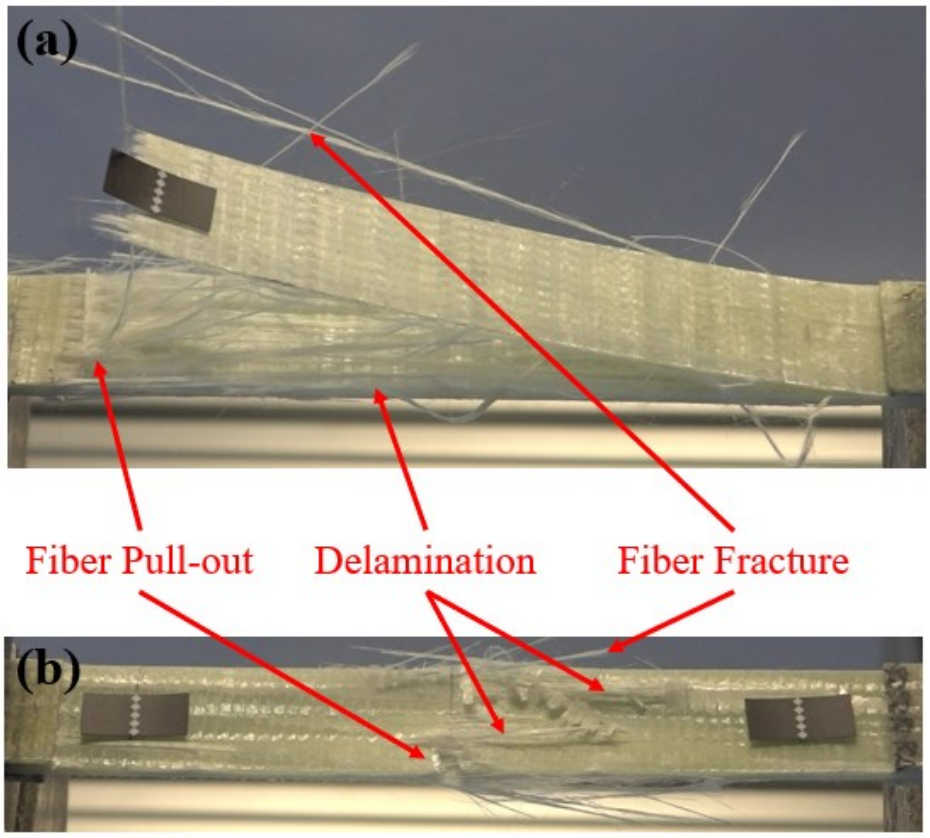

Figure 4.10. The deformed tensile test specimens (a) in the longitudinal and (b) in the transverse direction

4.2.3. V-notched Beam Test Results

The aim of the V-notched beam test was to determine the shear properties of the materials. The V-notched beam tests were performed in accordance with ASTM 5379M. The result obtained from the test is shown in Figure 4.11 while the failed specimen in this test is shown in Figure 4.12. From the result, the shear strength, shear modulus and shear strain in longitudinal, transverse and through-thickness directions were calculated as 50 MPa, 1.6 GPa and 0.075, respectively. It is found out that failure occurs because of pure shear stress between the notch roots, and the shear cracks propagate along the loading direction as shown in Figure 4.12. The results obtained from the V-notched beam test

shows similar values to the results obtained from the experimental study performed by Khashaba (Khashaba 2004).

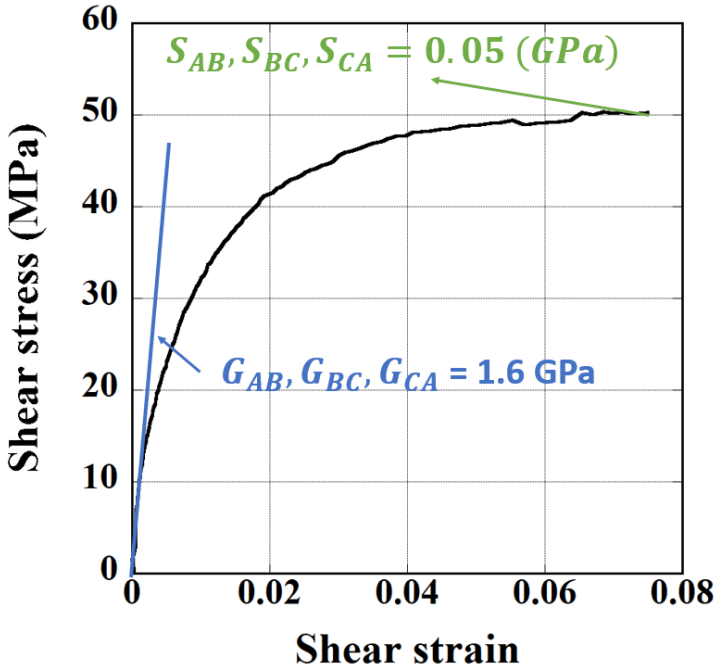

Figure 4.11. Shear stress versus shear strain of the E-Glass/composite materials

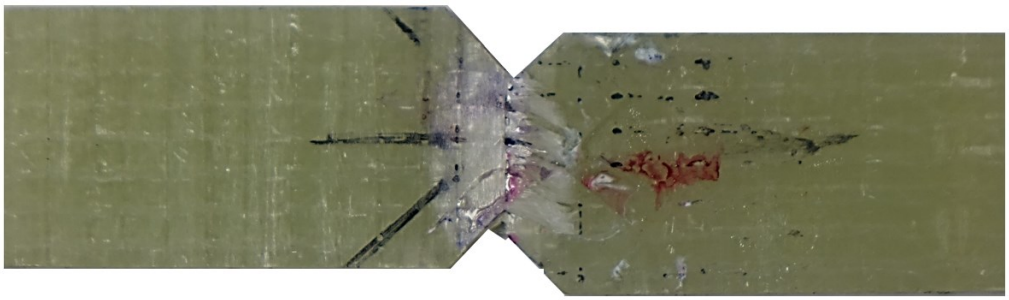

Figure 4.12. The failed V-notched beam test specimen

4.2.4. Laterally Constrained Compression Test Results

Laterally constrained compression tests were performed as described in the previous chapters. Fiber shear strength (SFS) and fiber crush strength (SFC) were determined. In this method, force was applied to the cubic specimen constrained laterally in the through-thickness direction. Then, the failed cubic sample at a shear angle of 44.3 degrees is shown in Figure 4.13. The stress versus time curves obtained from the four tests performed are shown in Figure 4.14. The fiber crush strength is calculated as 600 MPa from Figure 4.14. Using Equation 2.15 and the shear failure angle, 44.3°, the fiber shear strength was calculated as 290 MPa.

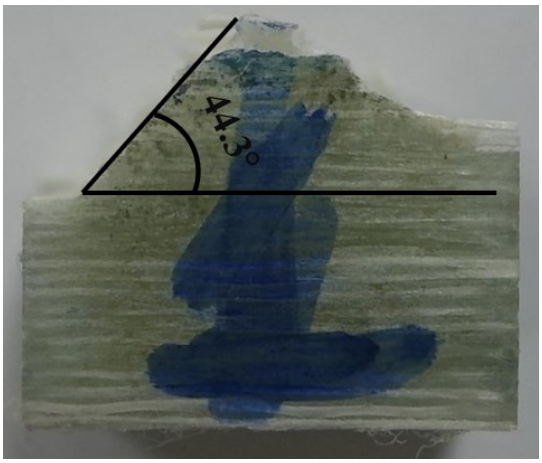

Figure 4.13. The failed cubic sample at a shear angle of 44.3 degrees in the laterally constrained compression test

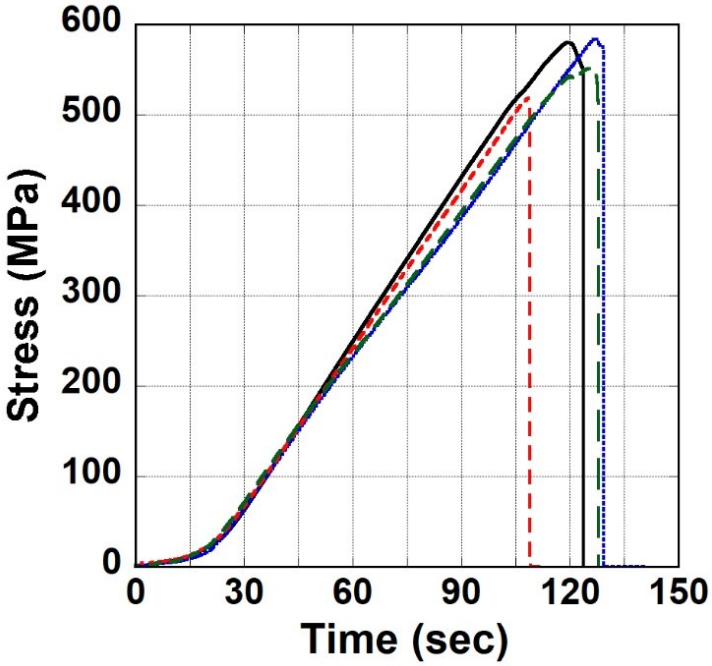

Figure 4.14. Laterally constrained test results

4.2.5. Elastic Constant Determination Test Results

Elastic constant determination tests were performed in the longitudinal and transverse directions. Force was applied to cubic specimens in these directions to determine their Poisson's ratios. The test results obtained are shown in Figure 4.15. In this figure, the Poisson's ratios are calculated as 0.21 for ϑ_{ca} and 0.247 for ϑ_{bc}.

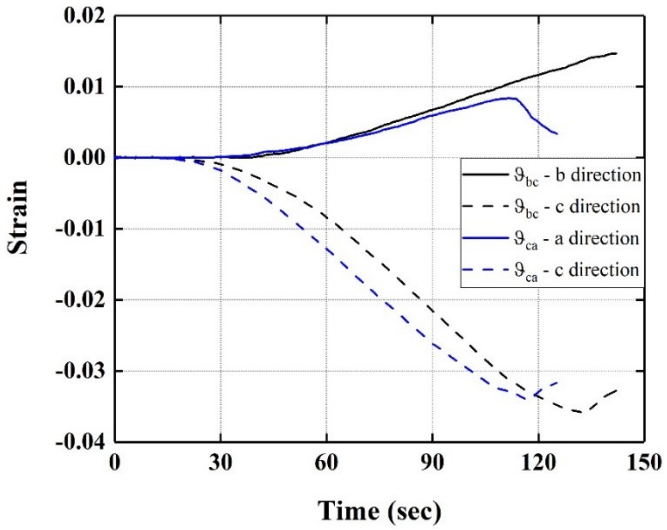

Figure 4.15. Elastic constant determination test results

4.2.6. Summarize of the Calibration Test Results

To determine MAT_162 material model parameters, quasi-static and dynamic tests were conducted according to the standard and non-standard test methods. The results obtained are summarized in Table 4.1. First, calibration models with the parameters in Table 4.1 are verified with the experimental studies. Then, multi-hit impact models with calibrated parameters are built for SHPB and projectile impact tests.

Table 4.1. The calibrated MAT_162 parameters

$\rho\ (kg\ m^{-3})$	1850	$E_{LIMT}, E_{EXPN}, E_{CRSH}$	1.5, 1.5, 0.001
$E_a, E_b, E_c\ (GPa)$	20, 20, 8.76	$S_{FC}\ (GPa)$	0.6
$\vartheta_{ab}, \vartheta_{bc}, \vartheta_{ca}$	0.13, 0.247, 0.21	$S_{AB}, S_{BC}, S_{CA}\ (GPa)$	0.05
$G_{AB}, G_{BC}, G_{CA}\ (GPa)$	1.6, 1.6, 1.6	$SFFC$	0.3
$S_{AT}, S_{BT}, (GPa)$	0.373, 0.368	$PHIC\ (deg)$	10
$S_{CT}\ (GPa)$	0.06	S_{DELM}	2.75
$S_{AC}, S_{BC}\ (GPa)$	0.352, 0.379	$S_{FS}\ (GPa)$	0.290
$AM1, AM2, AM3, AM4$	4.0, 4.0, 1.0, 0.3	C_1, C_2, C_3, C_4	0.0183, 0.001846, 0, 0.0163160

4.3. Experimental and Numerical Multi-hit Impact Test Results

In this section, the multi-hit impact test results obtained from numerical and experimental studies are presented, and the numerical ones are compared to the experimental ones.

4.3.1. Split Hopkinson Pressure Test Results

The experimental and numerical multi-hit impacts were only conducted for the composite samples in the through-thickness direction. An experimentally created incident stress wave was defined in the incident bar in the numerical model. Then this wave causes the incident bar to hit the transmitter bar at the same striker velocity. The results obtained from the first and second impact are interpreted in terms of stress versus time, stress versus strain and damage contours are shown in the following figures.

To determine the effect of the repeated loading on the residual strength of composite specimens, four tests were performed. The results are presented in Figure 4.16 and Figure 4.17 for the first and second impact. Test 1 is selected to further compare numerical results to experimental result.

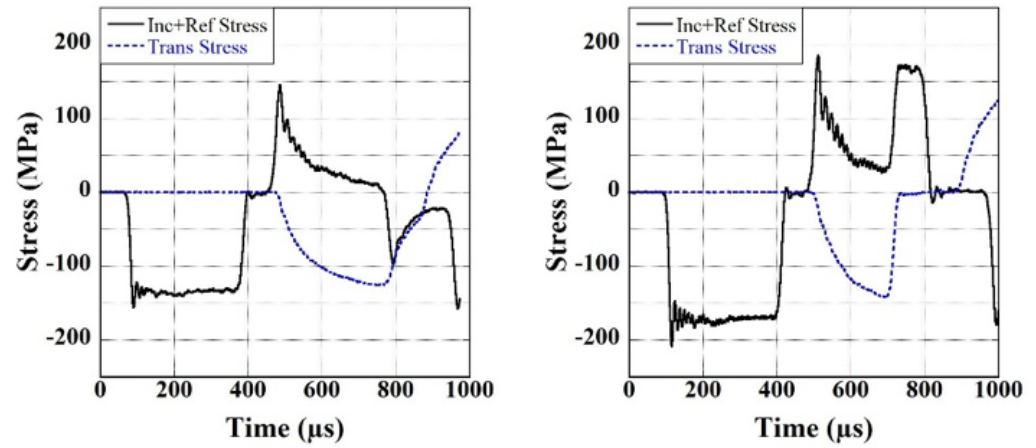

(a)

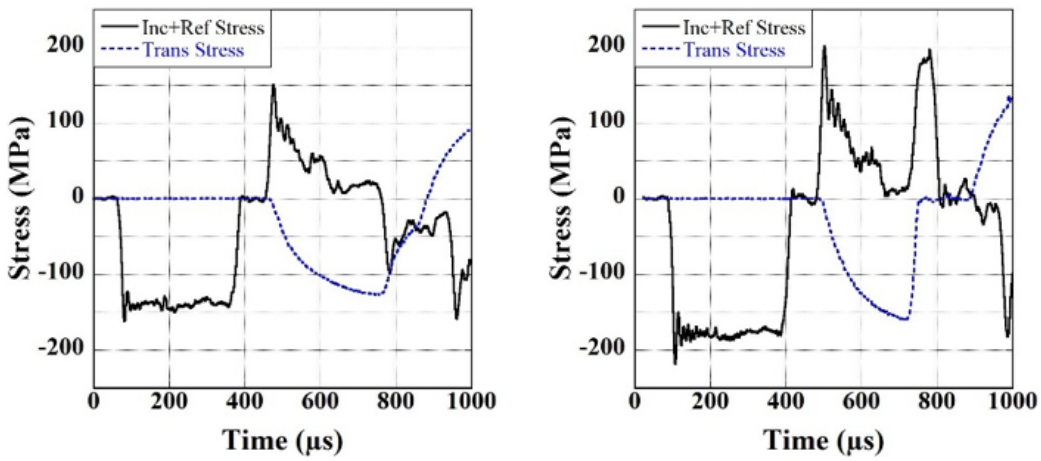

(b)

Figure 4.16. Bar response of the intact and damaged composite specimens obtained from experimental studies (a) Test 1 and (b) Test 2

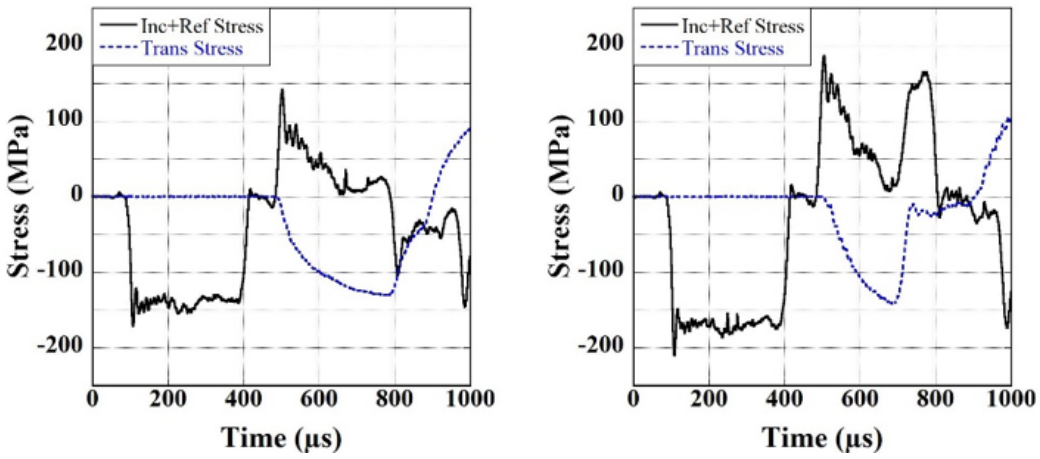

(a)

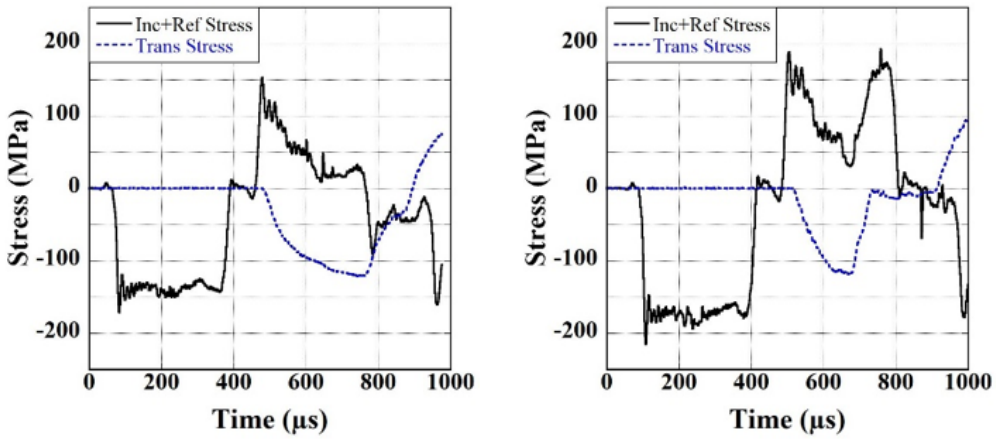

(b)

Figure 4.17. Bar response of the intact and damaged composite specimens obtained from experimental studies (a) Test 3 and (b) Test 4

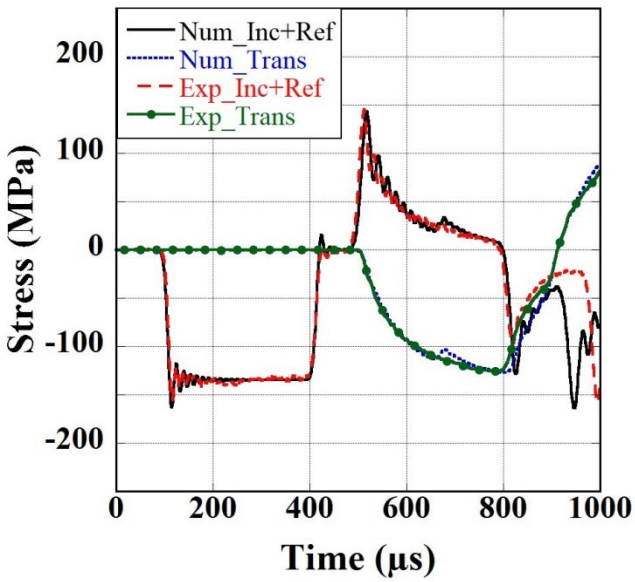

Figure 4.18. Bar response of the intact composite specimen obtained from the experimental and numerical study

The experimental and numerical stress pulses in the pressure bar as a function of time are illustrated in Figure 4.18, while the corresponding stress-strain rate-strain curves are depicted in Figure 4.19. The experiment and numerical stress pulses indicate that the amplitude of reflected stress wave reaches rapidly to its maximum value and then drops gradually to the zero. In the experimental and numerical stress-strain-strain rate curves, the deformation of the composite specimen occurs at nearly 330 s^{-1} strain rates. The stress value corresponding 0.058 and 0.061 strain is found as 460 MPa for both experimentally and numerically. These results show that numerical data well agree with the experimental data for the first impacting events.

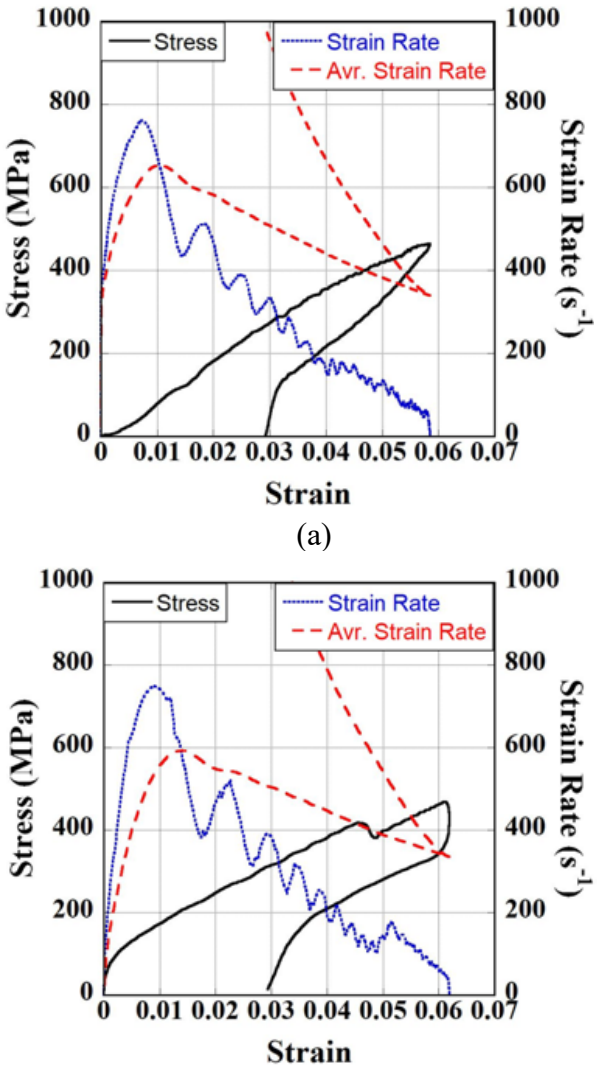

(a)

(b)

Figure 4.19. Stress-Strain Rate-Strain curves of the intact composite specimen (a) experiment and (b) numeric

For the first impact, the damage progression within the composite specimen in the through-thickness direction can be seen in Figure 4.20. High-speed video camera images are used to compare the deformation of the specimen with the numerically captured images. In this figure, damage development as a function of time is shown from undamaged specimen to the fully damaged specimen. In numerical simulation results, it is clearly seen that the delamination damage occurs at the interface between the first and second layer during the first impact. At the end of the analysis, this damage is concentrated between the layers at regions particularly close to the specimen-incident bar interface.

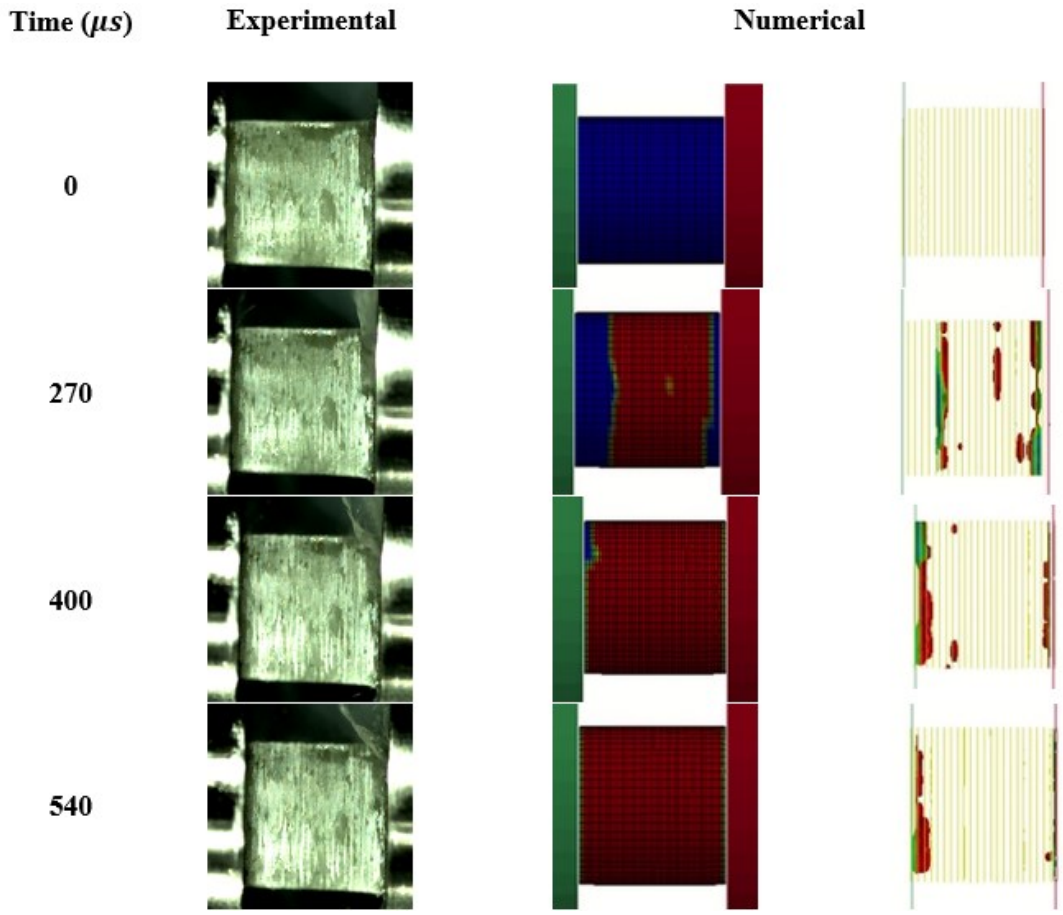

Figure 4.20. Damage sequences of the composite in through-thickness direction for the first impact both experimentally and numerically

The stress pulses and stress-strain-strain rate curves of the damaged specimen after the second impact are shown both experimentally and numerically in Figure 4.21 and Figure 4.22 respectively. Like the first impact on the intact specimen, the reflected pulse increases rapidly and decreases gradually in time, however, a sharp increase can be

seen at 700 µs. This shows that the failure of the specimen devastatingly takes place following that point. Correspondingly, the specimen fails in 520 MPa at 0.0069 strain in the experiment and 520 MPa at 0.006 strain in the numerical analysis. Strain rate is found as 469 s^{-1} and 524 s^{-1} for both experimental and numerical test, respectively. It is clearly seen that the numerical data well agree with the experimental data providing the validation and accuracy of the numerical model.

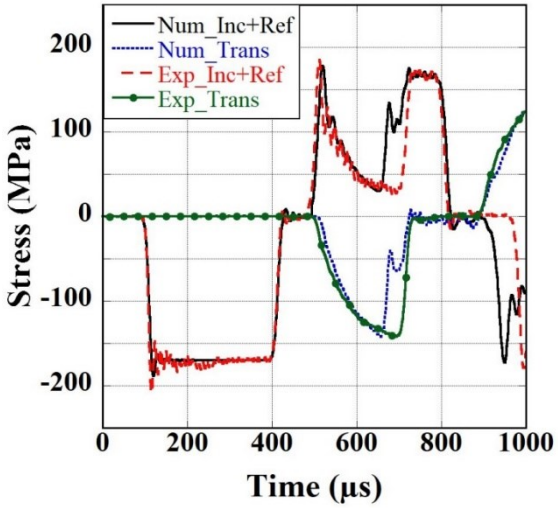

Figure 4.21. Bar response of the damaged composite specimen obtained from the experimental and numerical study

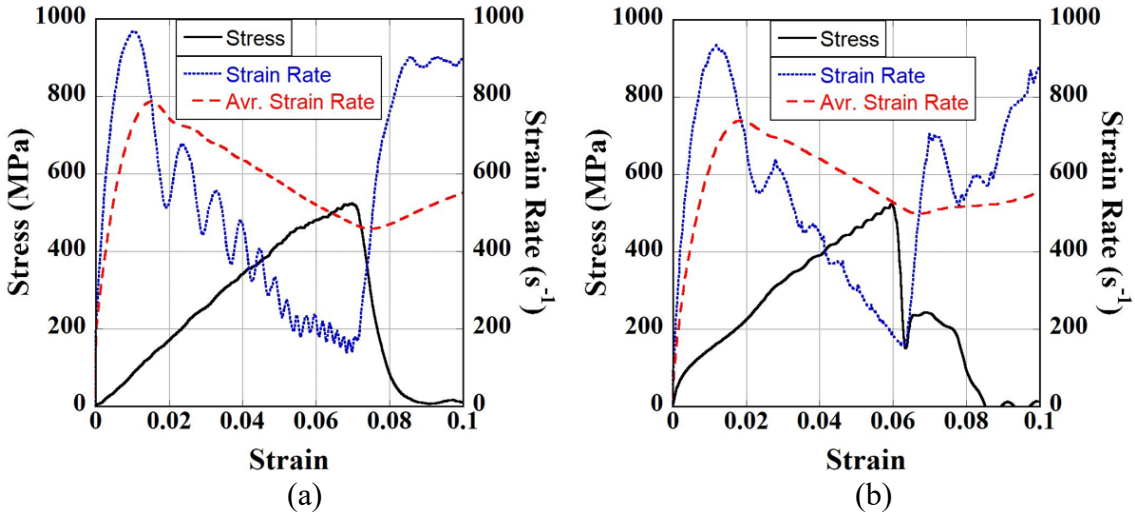

Figure 4.22. Stress-Strain Rate-Strain curves of the damaged composite specimen (a) experiment and (b) numeric

The images are obtained from experiments and numerical analysis during the second impact as shown in Figure 4.23. The damaged specimen is used as an input for

the second impact. It is clearly observed at the beginning of the second impact that there is some damage at the top part of the specimen at 0 μs. Therefore, the damage is successfully transferred from the first impact model to the second impact model using DYNAIN file method. This indicates that the method can be successfully used to model multiple impacts in LS-DYNA.

It is found out from the results in Figure 4.23 that after the composite specimen is subjected to the second impact, the delamination occurred at the first and second layer in the first impact propagates along the specimen-bar interfaces. In addition to that, the delamination is also observed at the interface between the eighth and ninth layer of the damaged specimen. Then, it failed devastatingly at 590 μs. When the experimental and numerical images are compared, delamination is found to be the main failure mode experimentally and numerically. Moreover, the specimen failed at 590 μs in the experimental study so did in the numerical study. Therefore, good agreements between them have been obtained.

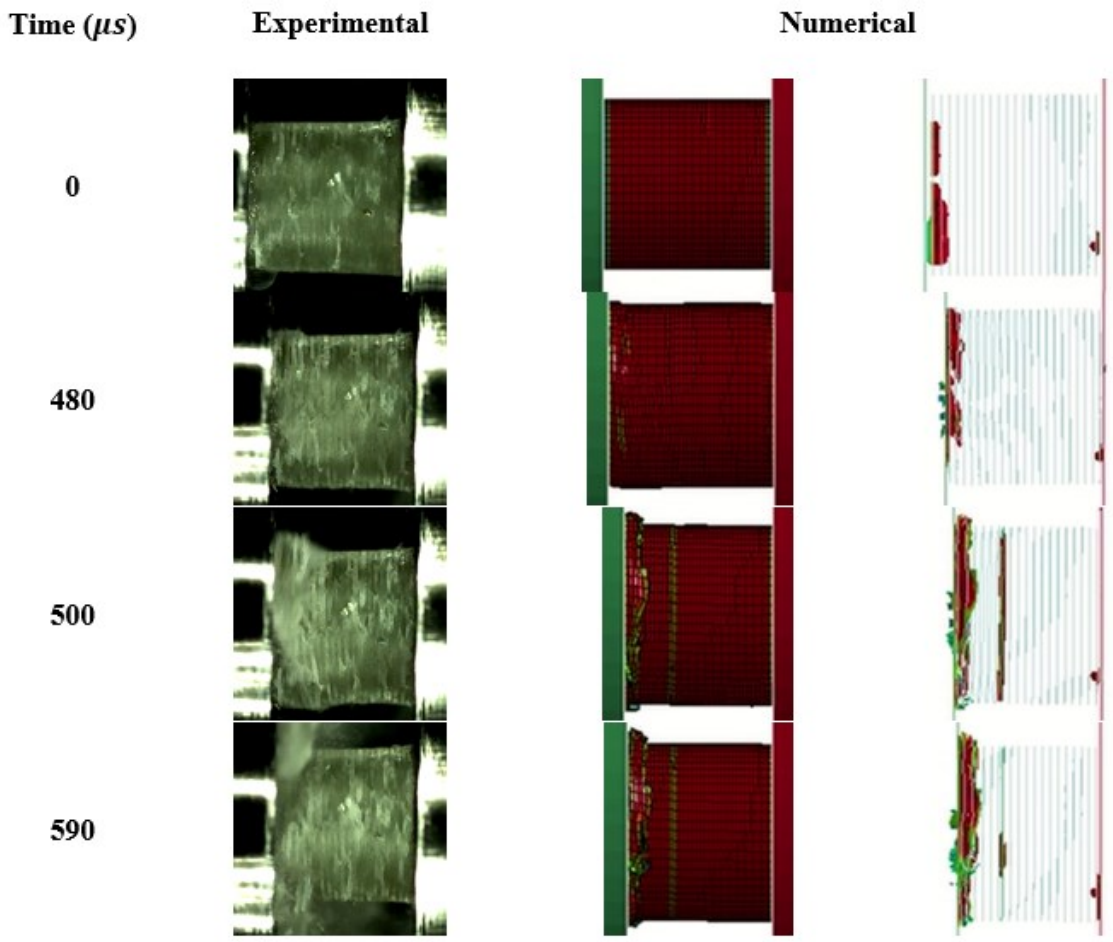

Figure 4.23. Damage sequences of the composite in through-thickness direction for the second impact both experimentally and numerically

4.3.2. Projectile Impact Test Results

To investigate the failure mechanism of composite laminates subjected to multi-hit impacts, the projectile was impacted on the same composite laminate in three times. The projectile velocity and dimensions were selected the same as in the experimental study. During tests, a high-speed video camera was used to record the deformation of the composite. Furthermore, the amount of delamination on the surface of the composite is measured after each impact and is summarized in Figure 4.24. After the first, second and third impact, the amount of delamination occurred on the front and back surface of the composites are 30.87 cm^2 and 180 cm^2 for the first impact, 55.75 cm^2 and 225 cm^2 for the second impact and 71.45 cm^2 and 225 cm^2. It can be easily seen that delamination on the back surface increase with increasing impact number until the third impact. The delamination does not propagate in the third impact since delamination spreads over the all back surface of the composite laminate in the second impact. At the front surface, the amounts of the delamination are lower than for those at the back surface, and the delamination increases with increasing impact number at the front face.

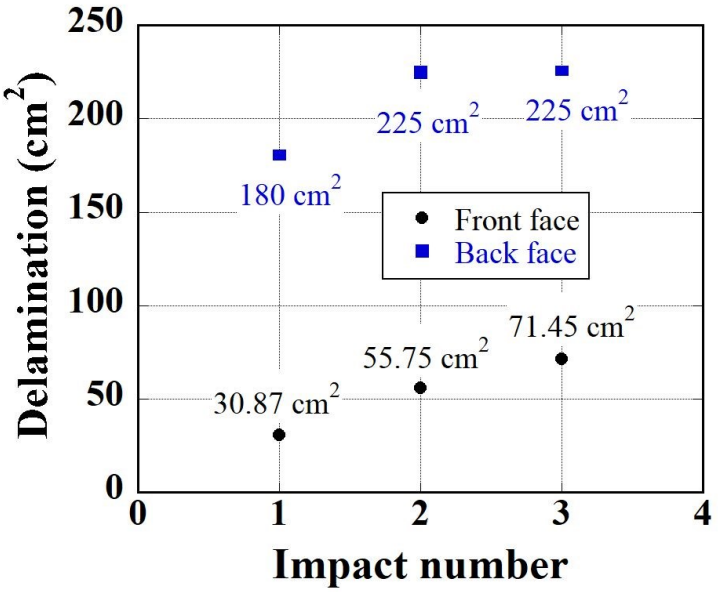

Figure 4.24. The amount of the delamination versus impact number curve

Kinetic energies of the projectile and contact forces at the different impact number are presented in Figure 4.25 (a) and (b) respectively. The kinetic energy of the projectile with an impact velocity of 130 m/s is calculated as 940 J for all the impact numbers. Then this amount is transferred to the composite laminate in 325 μs in the first impact, in 448

μs in the second and third impacts as shown in Figure 4.25 (a). When examined the contact force versus time curve (Figure 4.25 (b)) for all the impact numbers, it is found that the maximum contact force is 65 kN in the first impact, 44 kN in the second impact and 42 kN in the third impact. From these results, the contact force decreased with increasing number of impacts. Similar findings were also obtained by Haque et al. (Haque, Harrington, and Gillespie 2012b). The time required to reach the maximum contact force is 15 μs for the first impact, 32 μs for the second impact and 45 μs for the third impact. From these results, it can be understood that the time required to reach the maximum contact force increase with increasing impact numbers.

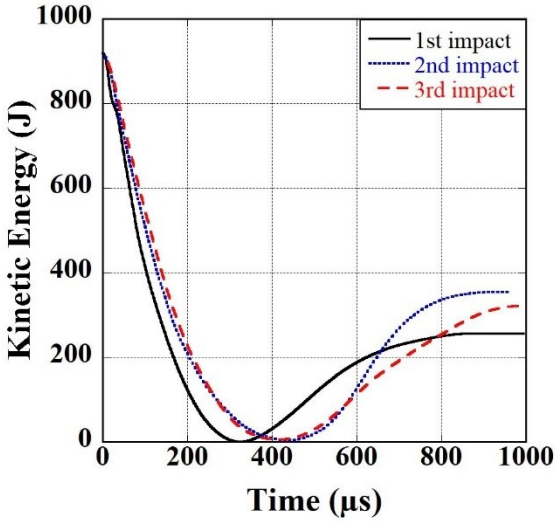

(a)

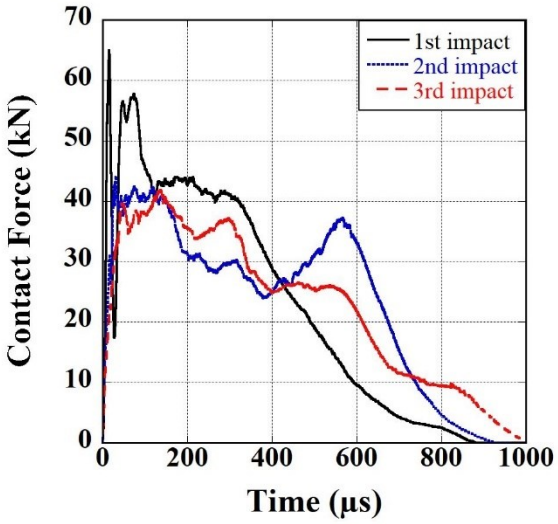

(b)

Figure 4.25. (a) Kinetic energies of the projectile versus time and (b) Contact forces versus time curves at different impacts

When the projectile begins to penetrate the composite material, delamination first occurs near the contact region, then propagates around the impact region. According to the experimental and numerical results in Figure 4.26, it is observed that during impacts, the front face of the composite is subjected to compression while its back face is subjected to tension. Thus, the amount of delamination on the front face is found to be less than on the back face. Due to the bending dominated tensile stress and reflections on the back face, matrix failure occurs and delamination propagates more areas. During penetration of the composite, delamination spreads out from the center point of the impact, and it is found to be more severe around this point on the front face.

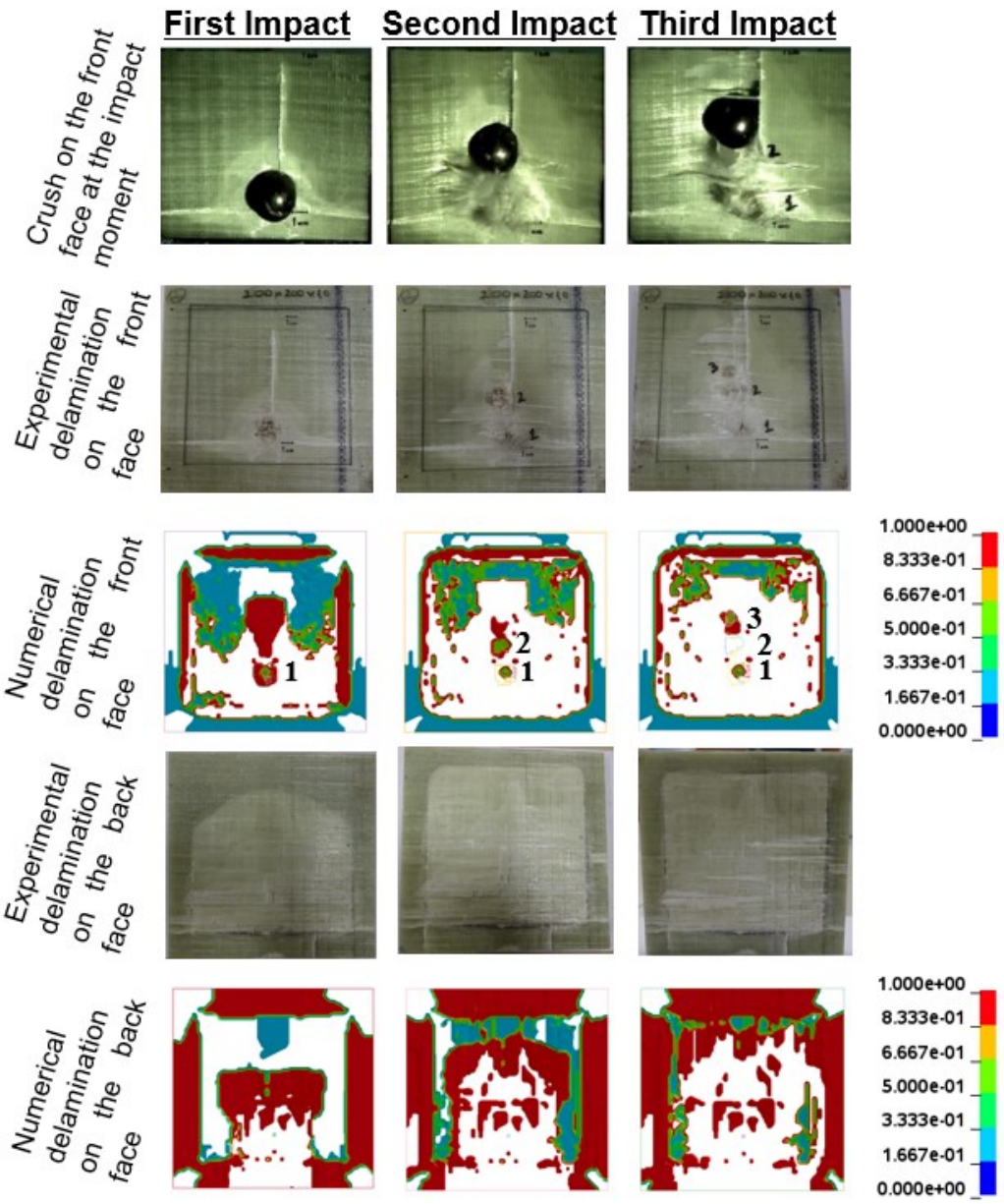

Figure 4.26. Delamination on the front and back face for each impact number

To validate the numerical model created using DYNAIN method, another numerical model was formed using Convetional method, and results obtained from DYAIN and Conventional method were compared with each other. Kinetic Energy and Contact Force results as a fuchtion of time for each impact case are prensented in Figure 4.27 and Figure 4.28, respectively.

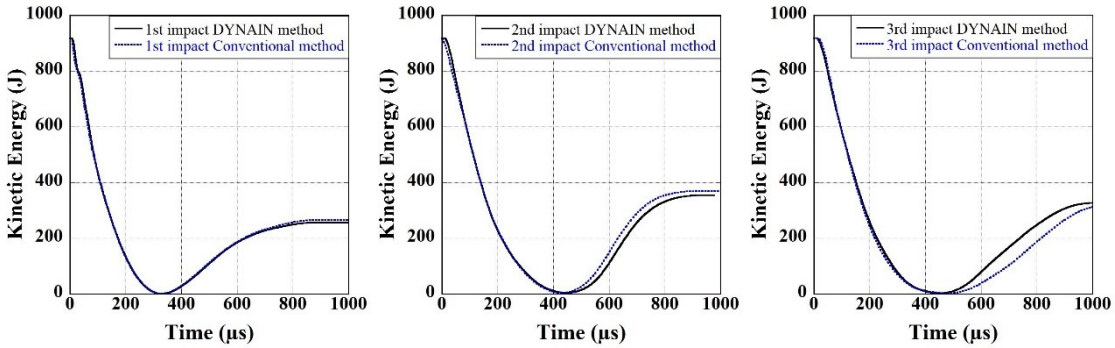

(a) (b) (c)

Figure 4.27. Kinetic Energy results of the numerical studies modeled using DYNAIN and Conventional method (a) for the first impact, (b) for the second impact and (c) for the third impact

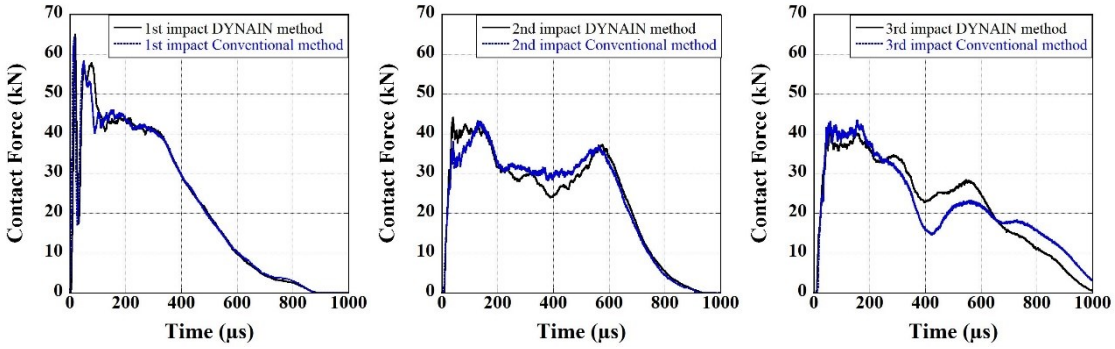

(a) (b) (c)

Figure 4.28. Contact Force results of the numerical studies modeled using DYNAIN and Conventional method (a) for the first impact, (b) for the second impact and (c) for the third impact

In Figure 4.27 (a) and Figure 4.28 (a), it can be shown for the first impact that the kinetic energy and contact force curves obtained by DYNAIN file method are nearly the same as those of the conventional method. The maximum contact force is determined for the both methods as 65 kN, and the required time to transfer all the kinetic energy of the projectile to the composite is determined as 325 µs for both methods. For the kinetic energy curves of the second and third impact, very similar kinetic energy curves are obtained by both the methods (Figure 4.27 (b) and (c)). All the kinetic energy of the

projectile is transferred to the composite in 448 μs for the second and third impact. After that time, the projectile begins to move in the opposite direction (+Z direction). In the second and third impact, the contact force and kinetic energy curves obtained from the DYNAIN file and conventional method shows slightly different behavior, as seen in Figure 4.28 (a) and (b). The reason for this difference is the positions of the composite laminate in DYNAIN file and conventional method, and the inertial kinetic energies. It demonstrates that the results obtained from DYNAIN file is safer than those of conventional method.

Table 4.2. Contour of history variables on the front surface of the composites modeled using DYNAIN file and Conventional method

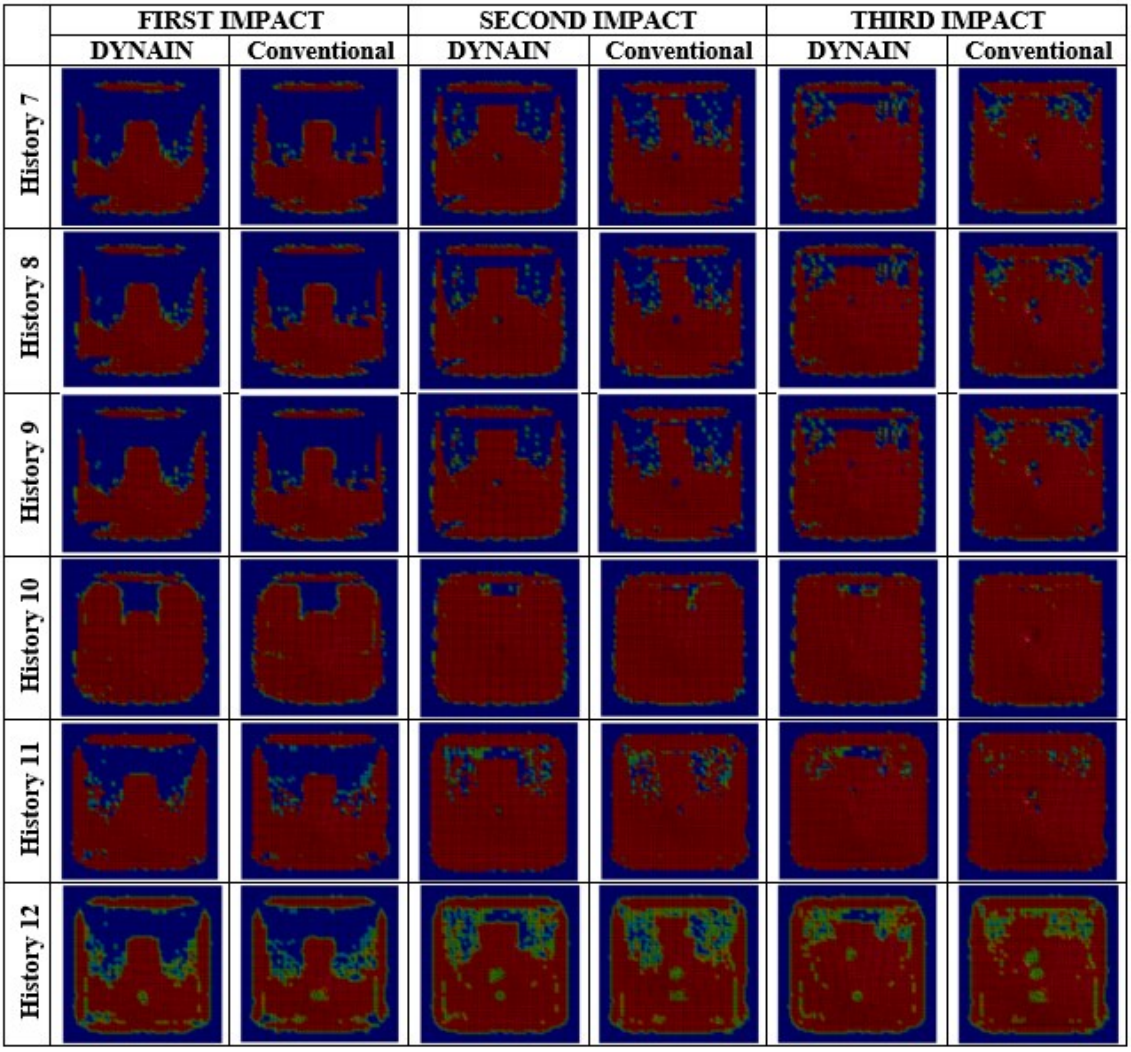

The numerical results obtained from DYNAIN and conventional method are presented in Table 4.2 for the front surface and in Table 4.3 for the back surface. Fiber

tension-shear damage mode along A and B directions (History 7 and History 8), fiber crush damage mode (History 9), in-plane matrix damage mode (History 10), transverse matrix damage mode (History 11) and delamination damage mode (History 12) within the composites modeled by DYNAIN file and conventional method are shown in these tables for each impact case. When comparing the damage modes obtained from DYNAN file and conventional method for each impact case, they are found be nearly the same. Besides it is clearly seen from these results that the damage on the front and back surface of the composites is properly transferred into the following impact models by using DYNAIN file method.

Table 4.3. Contour of history variables on the back surface of the composites modeled using DYNAIN file and Conventional method

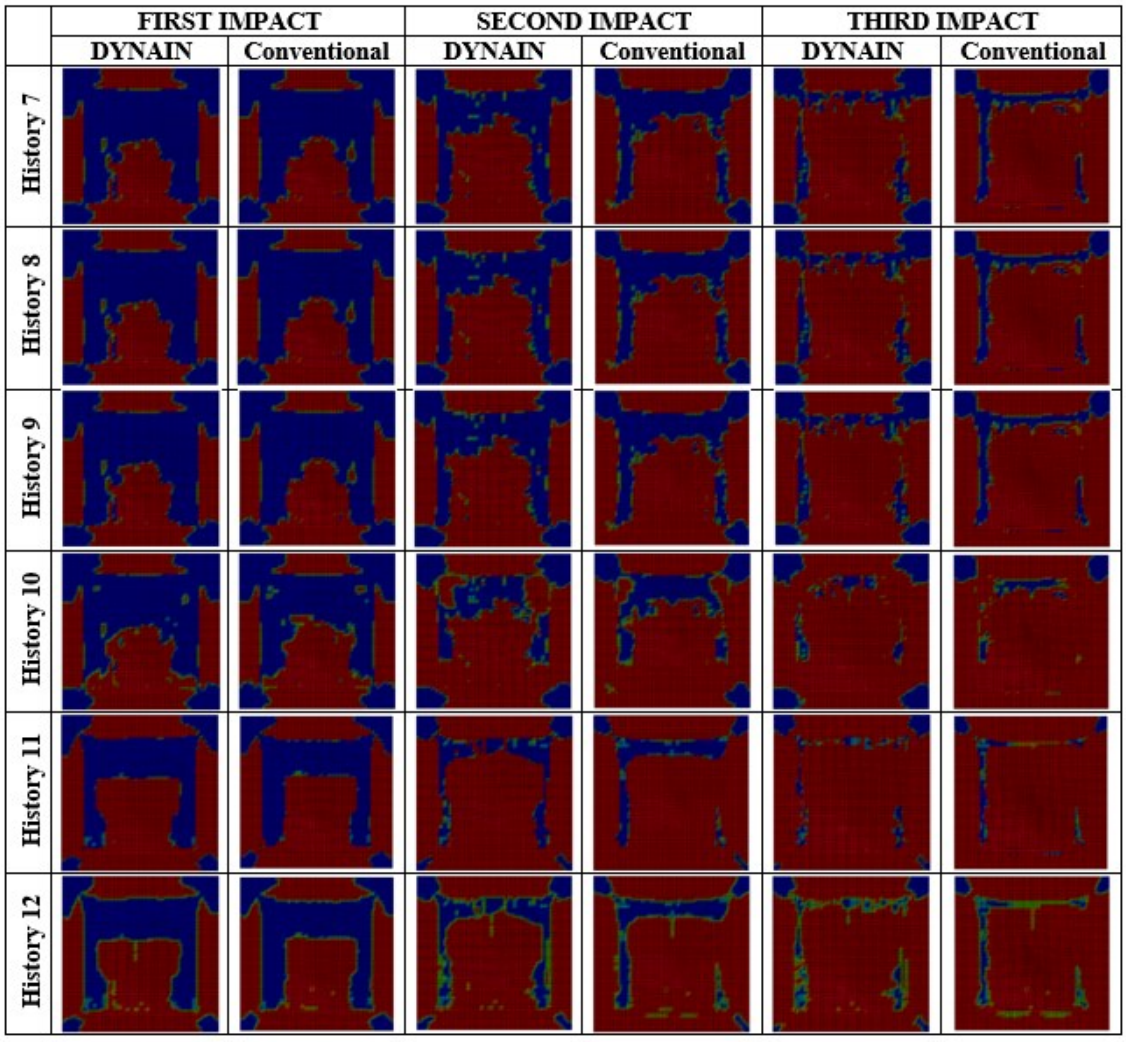

CHAPTER 5

CONCLUSIONS

Following results can be concluded;

- The compressive behavior of the composite in the transverse direction was found to have higher rate sensitivity than those longitudinal at high strain rates.
- The effect of strain rate on the compressive behavior was found to be more pronounced in the through-thickness direction.
- The samples in the in-plane directions split along the loading direction while those in the through-thickness matrix and fiber fracture was observed.

For the SHPB tests and models;

- Delamination was observed at the interface between the first and second layer, close to the specimen bar interface at the first hit. Then matrix damage was propagated along the interface, further delamination was also noted at the interface between the eighth and ninth layer of the composite ending with catastrophically failure after the second hit.
- The stress values recorded during the first loading were almost the similar levels for both experimental and numerical, while there was a slight deviation noted for the strain values.
- The stress values of the damaged composite specimen obtained experimentally and numerically were the same, but there were slight differences between strain and strain rate value.
- The reflected SHPB pulse recorded was increased from zero to a maximum value, then gradually decreased in the first hit proving that no catastrophic failure was occurred. However, a sharp rise was seen in the reflected pulse during the second hit indicating that significant amount of damage was imposed.

For the projectile impact tests and models;

- The amount of the delamination at the back face of the composite was higher than that of front face due to the bending dominated tensile stress and reflections at the free surface of the specimen.
- Most of the projectile kinetic energy (940 J) was transferred to the composite in the first 325 μs, while that value increased to 448 μs for the second and third hits.
- The contact force was decreased with increasing number of hits. This was occurred due to the fact that the stiffness of composite materials decreased with increasing number of impacts. The time corresponding to the maximum contact force increased as well.
- The results obtained from the numerical model following the conventional method showed similar results with the DYNAIN strategy in terms of damage formation, contact force and kinetic energy histories.

For future work, DYNAIN strategy can further be applied to multi-layer armor structures subjected to multi-hit impacts. Also, same strategy can be employed for modelling compression after impact (CAI) tests to determine the reductions in the strength of composite materials.

REFERENCES

Abir, M R, T E Tay, M Ridha, and H P Lee. 2017. "Modelling Damage Growth in Composites Subjected to Impact and Compression after Impact." *Composite Structures* 168: 13–25.

Abrate, Serge. 2011. *Impact Engineering of Composite Structures*. Vol. 526. Springer Science & Business Media.

An, Honggang, Daniel Green, Jennifer Johrendt, and Lorenzo Smith. 2013. "Multi-Objective Optimization of Loading Path Design in Multi-Stage Tube Forming Using MOGA." *International Journal of Material Forming* 6 (1): 125–35.

Arnold, W, and W Paul. 2001. "Behind Armor Debris Investigation and Their Application into a New Vulnerability Model." *International Journal of Impact Engineering* 26 (1–10): 21–32.

Arnold, W, and E Rottenkolber. 2003. "Behind Armor Debris Investigation - (Part II)." *International Journal of Impact Engineering* 29 (1–10): 95–104.

ASTM D5379. 2012. "Standard Test Method for Shear Properties of Composite Materials by the V-Notched." *Annual Book of ASTM Standards*.

ASTM International. 2017. "ASTM D3039 / D3039M-17, Standard Test Method for Tensile Properties of Polymer Matrix Composite Materials." *Standard Test Method for Tensile Properties of Polymer Matrix Composite Materials*.

Aurrekoetxea, J, M Sarrionandia, M Mateos, and L Aretxabaleta. 2011. "Repeated Low Energy Impact Behaviour of Self-Reinforced Polypropylene Composites." *Polymer Testing* 30 (2): 216–21.

Azouaoui, K, Z Azari, and G Pluvinage. 2010. "Evaluation of Impact Fatigue Damage in Glass/Epoxy Composite Laminate." *International Journal of Fatigue* 32 (2): 443–52.

Belingardi, Giovanni, Maria Pia Cavatorta, and Davide Salvatore Paolino. 2008. "Repeated Impact Response of Hand Lay-up and Vacuum Infusion Thick Glass Reinforced Laminates." *International Journal of Impact Engineering* 35 (7): 609–19.

Bors, Dana, Josh Cummins, and John Goodpaster. 2014. "The Anatomy of a Pipe Bomb

Explosion: The Effect of Explosive Filler, Container Material and Ambient Temperature on Device Fragmentation." *Forensic Science International* 234: 95–102.

Børvik, T, L Olovsson, A G Hanssen, K P Dharmasena, Håkan Hansson, and H N G Wadley. 2011. "A Discrete Particle Approach to Simulate the Combined Effect of Blast and Sand Impact Loading of Steel Plates." *Journal of the Mechanics and Physics of Solids* 59 (5): 940–58.

Briggs, Rachel E, Daniel R Drodge, David M Williamson, and William G Proud. 2007. "Two-Step Loading In A Split Hopkinson Pressure Bar." *AIP Conference Proceedings* 955 (1): 1173–76.

Caputo, F, A De Luca, G Lamanna, R Borrelli, and U Mercurio. 2014. "Numerical Study for the Structural Analysis of Composite Laminates Subjected to Low Velocity Impact." *Composites Part B-Engineering* 67: 296–302.

Caputo, F, A De Luca, and R Sepe. 2015. "Numerical Study of the Structural Behaviour of Impacted Composite Laminates Subjected to Compression Load." *Composites Part B-Engineering* 79: 456–65.

Chakraborty, Debabrata, and Munesh Kumar. 2005. "Response of Laminated FRP Composites under Multiple Impact Loading." *Journal of Reinforced Plastics and Composites* 24 (14): 1457–77.

Chen, W, and H Luo. 2004. "Dynamic Compressive Responses of Intact and Damaged Ceramics from a Single Split Hopkinson Pressure Bar Experiment." *Experimental Mechanics* 44 (3): 295–99.

Dathan, Jennifer. 2017. "Explosive Truths Monitoring Explosive Device in 2016." 2017. https://aoav.org.uk/wp-content/uploads/2017/05/AOAV-Explosive-Monitor-2017v9.pdf.

David-West, O S, D H Nash, and W M Banks. 2008. "An Experimental Study of Damage Accumulation in Balanced CFRP Laminates Due to Repeated Impact." *Composite Structures* 83 (3): 247–58.

Deka, L J, S D Bartus, and U K Vaidya. 2009. "Multi-Site Impact Response of S2-Glass/Epoxy Composite Laminates." *Composites Science and Technology* 69 (6): 725–35.

Denefeld, V, N Heider, A Holzwarth, A Sättler, and M Salk. 2014. "Reduction of Global Effects on Vehicles after IED Detonations." *Defence Technology* 10 (2):

219–25.

Fejdys, M, K Kosla, A Kucharska-Jastrzabek, and M Landwijt. 2016. “Hybride Composite Armour Systems with Advanced Ceramics and Ultra-High Molecular Weight Polyethylene (UHMWPE) Fibres.” *Fibres & Textiles in Eastern Europe* 24 (3): 79–89.

Found, M S, and I C Howard. 1995. “Single and Multiple Impact Behaviour of a CFRP Laminate.” *Composite Structures* 32 (1–4): 159–63.

Freitas, M De, and L Reis. 1998. “Failure Mechanisms on Composite Specimens Subjected to Compression after Impact.” *Composite Structures* 42 (4): 365–73.

Garzon-Hernandez, S, D Garcia-Gonzalez, and A Arias. 2018. “Multi-Impact Mechanical Behaviour of Short Fibre Reinforced Composites.” *Composite Structures*.

Ghelli, Daniele, and Giangiacomo Minak. 2011. “Low Velocity Impact and Compression after Impact Tests on Thin Carbon/Epoxy Laminates.” *Composites Part B: Engineering* 42 (7): 2067–79.

Greaves, Ian, and Paul Hunt. 2011. *Responding to Terrorism: A Medical Handbook*. Elsevier.

Han, G, Z D Guan, X Li, and S Y Du. 2016. “Failure Analysis of Carbon Fiber Reinforced Composite Subjected to Low Velocity Impact and Compression after Impact.” *Journal of Reinforced Plastics and Composites* 35 (9): 727–46.

Haque, B Z, J L Harrington, and J W Gillespie. 2012a. “Multi-Hit Ballistic Impact on S-2 Glass/SC15 Thick-Section Composites: Experiments.” *Journal of Strain Analysis for Engineering Design* 47 (7): 480–94.

Haque, B Z, J L Harrington, and J W Gillespie. 2012b. “Multi-Hit Ballistic Impact on S-2 Glass/SC15 Thick-Section Composites: Finite Element Analyses.” *Journal of Strain Analysis for Engineering Design* 47 (7): 495–512.

Hashin, Zvi. 1980. “Failure Criteria for Unidirectional Fiber Composites.” *Journal of Applied Mechanics* 47 (2): 329–34.

Hawyes, V J, P T Curtis, and C Soutis. 2001. “Effect of Impact Damage on the Compressive Response of Composite Laminates.” *Composites Part A: Applied Science and Manufacturing* 32 (9): 1263–70.

Hosur, M V, M R Karim, and S Jeelani. 2003. “Experimental Investigations on the Response of Stitched/Unstitched Woven S2-Glass/SC15 Epoxy Composites under Single and Repeated Low Velocity Impact Loading.” *Composite Structures* 61 (1–2): 89–102.

Jones, R. 1994. “Residual Strength of Composites with Multiple Impact Damage.” *Composite Structures* 28 (4): 347–56.

Jover, N, B Shafiq, and U Vaidya. 2014. “Ballistic Impact Analysis of Balsa Core Sandwich Composites.” *Composites Part B: Engineering* 67: 160–69.

Khashaba, U. A. 2004. “In-Plane Shear Properties of Cross-Ply Composite Laminates with Different off-Axis Angles.” *Composite Structures*.

Kong, X P, Z G Jiang, and F Liu. 2012. “Simulation on Ceramic Composite Armors against Multi-Hit of APPs.” In *Vibration, Structural Engineering and Measurement I, Pts 1-3*, edited by P P Lin and C L Zhang, 105–107:1648–+. Durnten-Zurich: Trans Tech Publications Ltd.

LSTC. 2015. “Ls-Dyna Keyword Users’S Manual.” In *LS-DYNA R8.0 Keyword User’s Manual - Volume II - Material Models*, 793–803.

Luo, H Y, W N W Chen, and A M Rajendran. 2006. “Dynamic Compressive Response of Damaged and Interlocked SiC-N Ceramics.” *Journal of the American Ceramic Society* 89 (1): 266–73.

Matzenmiller, ALJTR, J Lubliner, and R L Taylor. 1995. “A Constitutive Model for Anisotropic Damage in Fiber-Composites.” *Mechanics of Materials* 20 (2): 125–52.

Moorthy, T Nataraja, Mohamad Hadzri Yaacob, Reynold Vicente, and Mohd Taman. 2014. “A Study into the Relationship between Crater Parameters and Quantities of Explosives in the Scenes of IED Explosions.” *Malaysian Journal of Forensic Sciences: Mission Statement* 5 (1): 17–25.

Morais, W A De, S N Monteiro, and J R M d’Almeida. 2005a. “Effect of the Laminate Thickness on the Composite Strength to Repeated Low Energy Impacts.” *Composite Structures* 70 (2): 223–28.

Morais, W A De, S N Monteiro, and J R M d’Almeida. 2005b. “Evaluation of Repeated Low Energy Impact Damage in Carbon–epoxy Composite Materials.” *Composite*

Structures 67 (3): 307–15.

Mouritz, A P, J Gallagher, and A A Goodwin. 1997. “Flexural Strength and Interlaminar Shear Strength of Stitched GRP Laminates Following Repeated Impacts.” *Composites Science and Technology* 57 (5): 509–22.

Mukherjee, Sourish, Rittik Bhowmik, Aparna Das, and Sulagno Banerjee. 2017. “Review Paper On Blast Loading And Blast Resistant Structures.” *International Journal of Civil Engineering and Technology* 8 (8): 988–96.

Naebe, M, J Sandlin, I Crouch, and B Fox. 2013. “Novel Polymer-Ceramic Composites for Protection against Ballistic Fragments.” *Polymer Composites* 34 (2): 180–86. https://doi.org/10.1002/pc.22397.

Naik, N K, M N Joglekar, H Arya, S V Borada, and K N Ramakrishna. 2004. “Impact and Compression after Impact Characteristics Ofplain Weave Fabric Composites: Effect of Plate Thickness.” *Advance Composite Materials* 12 (4): 261–80.

Olovsson, L, A G Hanssen, T Borvik, and M Langseth. 2010. “A Particle-Based Approach to Close-Range Blast Loading.” *European Journal of Mechanics A-Solids* 29 (1): 1–6.

Perez-Martin, M J, A Enfedaque, W Dickson, and F Galvez. 2012. Impact Behaviour Of Hybrid Glass/Carbon Epoxy Composites. Edited by M Wickert and M Salk. *27th International Symposium on Ballistics, Vols. 1 and 2*. Lancaster: Destech Publications, Inc.

Prakash, A, S M Srinivasan, and A R M Rao. 2017. “Response of Steel Fiber Reinforced Cementitious Composite Panels Subjected to Extreme Loading Conditions.” *Journal of Engineering Materials and Technology-Transactions of the Asme* 139 (2): 7.

Remacha, M, S Sanchez-Saez, B Lopez-Romano, and E Barbero. 2015. “A New Device for Determining the Compression after Impact Strength in Thin Laminates.” *Composite Structures* 127: 99–107.

Rottenkolber, E, and W Arnold. 2006. “Physics of behind Armor Debris Threat Reduction.” *International Journal of Impact Engineering* 33 (1–12): 53–61.

Sanchez-Saez, S, E Barbero, R Zaera, and C Navarro. 2005. “Compression after Impact of Thin Composite Laminates.” *Composites Science and Technology* 65 (13):

Shim, V P W, J Yuan, and S H Lee. 2001. “A Technique for Rapid Two-Stage Dynamic Tensile Loading of Polymers.” *Experimental Mechanics* 41 (1): 122–27.

Singh, Ajay K, Noah G Ditkofsky, John D York, Hani H Abujudeh, Laura A Avery, John F Brunner, Aaron D Sodickson, and Michael H Lev. 2016. “Blast Injuries: From Improvised Explosive Device Blasts to the Boston Marathon Bombing.” *Radiographics* 36 (1): 295–307.

Sugun, B S, and RMVGK Rao. 2004. “Low-Velocity Impact Characterization of Glass, Carbon and Kevlar Composites Using Repeated Drop Tests.” *Journal of Reinforced Plastics and Composites* 23 (15): 1583–99.

Tasdemirci, A, A Kara, K Turan, and S Sahin. 2015. “Dynamic Crushing and Energy Absorption of Sandwich Structures with Combined Geometry Shell Cores.” *Thin-Walled Structures* 91: 116–28.

Tasdemirci, Alper, Selim Sahin, Ali Kara, and Kivanc Turan. 2015. “Crushing and Energy Absorption Characteristics of Combined Geometry Shells at Quasi-Static and Dynamic Strain Rates: Experimental and Numerical Study.” *Thin-Walled Structures* 86: 83–93.

U.S. Department of Homeland Security Office for Bombing Prevention. 2018. “IED and Explosive Effects Fundamental.” Vol. 2018.

Xia, K, R Chen, S Huang, and S N Luo. 2008. “Controlled Multipulse Loading with a Stuffed Striker in Classical Split Hopkinson Pressure Bar Testing.” *Review of Scientific Instruments* 79 (5).

Xiong, Y, C Poon, P V Straznicky, and H Vietinghoff. 1995. “A Prediction Method for the Compressive Strength of Impact Damaged Composite Laminates.” *Composite Structures* 30 (4): 357–67.

Yan, Hao, Caglar Oskay, Arun Krishnan, and Luoyu Roy Xu. 2010. “Compression-after-Impact Response of Woven Fiber-Reinforced Composites.” *Composites Science and Technology* 70 (14): 2128–36.

Yarin, A L, I V Roisman, K Weber, and V Hohler. 2000. “Model for Ballistic Fragmentation and Behind-Armor Debris.” *International Journal of Impact Engineering* 24 (2): 171–201.

Yen, Chian-Fong. 2012. “A Ballistic Material Model for Continuous-Fiber Reinforced Composites.” *International Journal of Impact Engineering* 46 (August): 11–22.